

Multimodal AI predicts clinical outcomes of drug combinations from preclinical data

Yepeng Huang^{1,2}, Xiaorui Su^{1,*}, Varun Ullanat^{1,*}, Ivy Liang³, Lindsay Clegg⁴, Damilola Olabode⁵, Nicholas Ho⁶, Bino John⁷, Megan Gibbs⁵, and Marinka Zitnik^{1,8,9,10,‡}

¹Department of Biomedical Informatics, Harvard Medical School, Boston, MA

²Program in Biological and Biomedical Sciences, Harvard Medical School, Boston, MA

³Harvard College, Cambridge, MA

⁴Clinical Pharmacology and Quantitative Pharmacology, Clinical Pharmacology & Safety Sciences, R&D, AstraZeneca, Gaithersburg, MD

⁵Clinical Pharmacology and Quantitative Pharmacology, Clinical Pharmacology & Safety Sciences, R&D, AstraZeneca, Waltham, MA

⁶Program in Computational Biology, Carnegie Mellon University, Pittsburgh, PA

⁷Imaging and Data Analytics, Clinical Pharmacology & Safety Sciences, R&D, AstraZeneca, Waltham, MA

⁸Kempner Institute for the Study of Natural and Artificial Intelligence, Harvard University, Allston, MA

⁹Broad Institute of MIT and Harvard, Cambridge, MA

¹⁰Harvard Data Science Initiative, Cambridge, MA

*Co-second authors

‡Corresponding author: marinka@hms.harvard.edu

Predicting clinical outcomes from preclinical data is essential for identifying safe and effective drug combinations, reducing late-stage clinical failures, and accelerating the development of precision therapies. Current models rely on structural or target-based features to identify high-efficacy, low-toxicity drug combinations. However, these approaches fail to incorporate the multimodal data necessary for accurate, clinically-relevant predictions. Here, we introduce MADRIGAL, a multimodal AI model that learns from structural, pathway, cell viability, and transcriptomic data to predict drug combination effects across 953 clinical outcomes and 21,842 compounds, including combinations of approved drugs and novel compounds in development. MADRIGAL uses a transformer bottleneck module to unify preclinical drug data modalities while handling missing data during training and inference—a major challenge in multimodal learning. It outperforms single-modality methods and state-of-the-art models in predicting adverse drug interactions. MADRIGAL performs virtual screening of anticancer drug combinations and supports polypharmacy management for type II diabetes and metabolic dysfunction-associated steatohepatitis (MASH). It identifies transporter-mediated drug interactions. MADRIGAL predicts resmetirom, the first and only FDA-approved drug for MASH, among therapies with the most favorable safety profile. It supports personalized cancer therapy by integrating genomic profiles from cancer patients. Using primary acute myeloid leukemia samples and patient-derived xenograft models, it predicts the efficacy of personalized drug combinations. Integrating MADRIGAL with a large language model allows users to describe clinical outcomes in natural language, improving safety assessment by identifying potential adverse interactions and toxicity risks. MADRIGAL provides a multimodal approach for designing combination therapies with improved predictive accuracy and clinical relevance.

Main

Combination therapies improve clinical outcomes by enhancing efficacy and reducing adverse effects through lower doses or complementary mechanisms [1–3]. While drug combinations can enhance treatment efficacy, they also elevate the risk of adverse drug reactions due to drug-drug interactions (DDIs). For example, the combination of infliximab and azathioprine has been shown to be more effective than monotherapy in inducing and maintaining corticosteroid-free remission in Crohn’s disease, but has also been shown to be associated with infections and other adverse effects [4]. Similarly, combining nivolumab with chemotherapy has improved overall survival in advanced esophageal squamous cell carcinoma, yet this approach is associated with higher incidences of treatment-related adverse events [5]. These interactions can pose significant risks for vulnerable populations such as cancer survivors [6], patients with chronic [7] and neurological diseases [8]. Despite the potential of combination therapies, identifying clinically effective and safe drug combinations remains challenging due to the overwhelming number of possible drug pairings and the heterogeneity of clinical effects [9, 10].

A major challenge in predicting drug combination effects for novel compounds—those in preclinical or early clinical development—is the absence of critical data that emerge only in later stages. These missing data, including clinical safety profiles, long-term efficacy, and pharmacokinetics, constrain accurate prediction of drug interactions and therapeutic effects. Accurately predicting drug combinations with limited preclinical data is thus essential for improving clinical success rates [11], reducing patient risk and prevent unnecessary clinical investigations.

Various preclinical data modalities provide insight into the clinical effects of drug combinations, including molecular structures, mechanisms of action, and perturbation outcomes from cell-based assays. Although molecular structure is universally available and provides insights into drug bioactivity [12, 13], it is often insufficient for characterizing drug combinations. This limitation arises from complex pharmacodynamic interactions that extend beyond molecular properties [14] (Supplementary Fig. S1a) and requires a broader understanding of drug action [15]. Perturbation-based modalities include transcriptional changes in cell lines [16] and cell viability profiles [17] following chemical perturbations, which can be measured at high throughput [16] and capture complex biological responses to drugs [18–20]. Despite their relevance, perturbation data remain underutilized in predictive modeling, yet they are essential for understanding drug synergy and safety [21, 22]. Transcriptional phenotypes provide readouts of drug-protein interactions and pathway-level changes in cellular activity [23–26]. Cell viability data reveal how drugs influence signaling pathways across tissues and cell types, enabling the identification of gene functions relevant to drug action [27–29]. This is critical for target

prioritization [30], detecting adverse drug interactions [31–33], and managing polypharmacy in patients with comorbidities.

A key barrier to utilizing preclinical data to achieve accurate prediction of drug combination clinical outcomes is the “missing modality” problem [34–36] (Fig. 1c), where crucial data are unavailable for novel compounds in preclinical stages and even for some approved drugs. Approaches that assume complete data availability during training cannot leverage drugs with incomplete modality profiles. This disproportionately affects novel compounds lacking pathway annotations and early-stage experimental drugs with sparse toxicity data. To address this, there is a need for multimodal AI models that can handle missing modalities at both training and inference stages of AI modeling.

Here, we introduce MADRIGAL, a multimodal AI model that predicts drug combination outcomes. MADRIGAL unifies drug structural, pathway, cell viability, and transcriptomic modalities throughout the AI model, including combinations of compounds that lack preclinical data modalities or reported clinical efficacy and safety data (Fig. 1c). By aligning modality-specific drug representations using contrastive learning [37, 38], MADRIGAL learns a unified multimodal latent space for improved performance across clinical outcomes and can be integrated with large language models (LLMs) to model outcomes beyond those included in predefined medical vocabularies and standardized ontologies. We use MADRIGAL to evaluate new and approved cancer combination therapies involving poly (ADP-ribose) polymerase inhibitors (PARPi), including olaparib, talazoparib, and rucaparib. MADRIGAL predicts olaparib + abiraterone to have a more favorable safety profile than olaparib + paclitaxel, based on lower predicted adverse effect score (a “favorable safety profile” is defined based on predicted score of adverse effects). Beyond cancer treatments, we also evaluated MADRIGAL predictions for treating chronic metabolic disorders, resulting in insights into complex drug regimens used in type II diabetes and metabolic dysfunction-associated steatohepatitis (MASH). MADRIGAL supports personalized cancer therapy by predicting effective drug combinations using patient genomic profiles from primary acute myeloid leukemia samples [39, 40] and patient-derived tumor xenografts [41]. It identifies responders by modeling drug synergy and treatment response across diverse genetic backgrounds.

Results

MADRIGAL multimodal AI model for predicting drug combination outcomes.

Predicting effective combination therapies requires models that can generalize across diverse data modalities available. Existing approaches often assume complete modality data

during both training and inference, limiting their applicability when certain modalities are missing—a common challenge in preclinical and clinical studies. This constraint is particularly problematic for predicting drug combination outcomes, as information on novel or experimental compounds is often sparse. MADRIGAL is a universal multimodal model designed to handle incomplete modality inputs during both training and inference. It predicts clinical outcomes and adverse reactions of drug combinations using preclinical data, supporting decision-making for both existing combination therapies and novel drug candidates. Using structural drug information, molecular pathways knowledge graph, transcriptomic responses, and cell viability data, it predicts combination therapy effects across 953 outcomes (Fig. 1a,b, such as “increase in QTc prolongation”) and through integration with an LLM, MADRIGAL-LLM extends to free text descriptions of outcomes beyond codified clinical vocabularies (Fig. 6a).

For each pair of drugs, MADRIGAL processes available modality inputs individually via modality-specific encoders, mapping each modality to a unified embedding space. These modality-specific embeddings function as tokens (vector representations of input data) that are fed into a fusion module comprising multiple customized transformer encoder layers, concluding with a cross-attention layer (Supplementary Fig. S1b). Bottleneck tokens are placed between structure, pathway, cell viability, and transcriptomic modality tokens, balancing information from the distinct transcriptomic responses of each cell line [42]. The fusion module generates a single embedding by applying cross-attention between a summarization query token and the bottleneck tokens from the last transformer encoder block [43, 44]. The resultant multimodal embedding for each drug, when paired and passed through a decoder module, outputs a final predicted score for each outcome (Fig. 1b, Supplementary Fig. S1b).

To ensure alignment between data modalities, MADRIGAL uses contrastive pretraining to align modality-specific embeddings with the structure modality, the only universal data type available for all small molecule compounds (Fig. 1a,c). After alignment, MADRIGAL generates unified representations in latent space, allowing for fine-tuning of drug combination datasets (formatted as [drug 1, drug 2, outcome]; Methods Sec. 2) (Fig. 1d, Supplementary Fig. S1a).

Evaluating MADRIGAL across drug combination prediction tasks.

We first evaluated MADRIGAL on tasks in which (1) all samples involving a specific drug combination (“split-by-drug pairs”) or (2) all samples involving a specific drug (along with its combinations) were held out during training (“split-by-drugs”). The latter scenario better simulates the cases where the outcomes need to be predicted for a novel compound combined with an approved drug, as the drug that is held out mimics new compounds not encountered by the model during training (Fig. 2a).

MADRIGAL model is trained on the following two datasets: TWO SIDES (2019-11-15), a self-reported DDI dataset extracted from FDA Adverse Event Reporting System (FAERS) [45] containing 4,656,138 drug combinations across 1,457 drugs and 795 outcomes, and DrugBank (2023-01-04), an expert-curated dataset with 1,188,371 drug combinations involving 3,632 drugs and 158 outcomes [46] (Methods Sec. 1). To test MADRIGAL’s generalizability, we created several dataset splits: in addition to random splits by drug pairs or drugs, we designed two splits to test model generalization. In the split-by-drugs (target) approach, the drugs in the test set have none or only a few therapeutic targets in common with those in the training set. In the split-by-drugs (ATC) approach, drugs from specific first level categories within the Anatomical Therapeutic Chemical (ATC) classification system were excluded from the training set (Methods Sec. 1). These splits significantly increased structural differences between training and test drugs compared to random splits (Supplementary Fig. S2a). For each dataset and splitting strategy, models are trained separately on the respective dataset and split for evaluation. Unless otherwise specified, the model trained on the full DrugBank dataset is used for pharmacological applications throughout this paper.

These dataset splits reflect challenges in drug combination development, where novel compounds are developed for new targets, often with limited preclinical data. While models have performed well on typical drug combination benchmarks [45–47], they usually assume all possible drugs have been encountered during training, an assumption that does not match scenarios in which new compounds are paired with existing drugs. For example, an approved drug may be combined with a novel compound to mitigate safety issues, enhance efficacy, or expand the approved drug’s indications. The ability to model interactions with such novel compounds early in development, when only limited preclinical data is available, could streamline the development of combination therapies [11].

In our comparisons, we included state-of-the-art models categorized by data modalities: chemical structure-based models (DeepDDI [48], CASTER [49], GMPNN-CS [50]) that capture molecular structure through learning on molecular graphs; knowledge graph (KG)-based models (DDKG [51]) that capture drug mechanism of action and include information on targets, enzymes, transporters, drug indications, and adverse effects; and multimodal models (MUFFIN [52], TIGER [53]). These models use either late fusion [51–53]—where each drug molecule is encoded separately and merged—or early fusion, where molecular interactions are modeled from the start [48–50]. For evaluation metrics, we used the area under the receiver-operating curve (AUROC), the area under the precision-recall curve (AUPRC), and the maximum F measure (Fmax) (Methods Sec. 3.1). To further reflect drug combination development

when information is limited for novel compounds, we restricted MADRIGAL’s input during testing to only those modalities typically available preclinically (Fig. 2a). In contrast, baselines were provided with full multimodal inputs. This deliberate limitation makes the prediction task more challenging for MADRIGAL.

MADRIGAL predicts multimodal drug combination safety.

MADRIGAL demonstrated strong performance across both datasets, various types of splitting, and evaluation metrics (split-by-drugs (target) setting in Fig. 2b, split-by-drugs (ATC, random) and split-by-drug pairs settings in Supplementary Fig. S3). While GMPNN-CS matched MADRIGAL’s AUROC (+0.001) in DrugBank (split-by-drugs target) and CASTER excelled in split-by-drug pairs, MADRIGAL was the most reliable overall, particularly in challenging scenarios.

In the split-by-drugs (target) setting, MADRIGAL demonstrated an average improvement of 10.7% across all metrics compared to structure-based models on TWOSIDES. Similarly, on DrugBank, MADRIGAL outperformed most structure-based models across all metrics by, on average, 6.2% (Fig. 2b). Although CASTER and GMPNN-CS utilize explicit substructure learning strategies and employ early fusion to enable information flow between drugs early on, MADRIGAL adopts a late fusion strategy, first integrating multiple modalities for each compound before combining the drug representations, all while using a simple lightweight structural encoder. The superior performance of MADRIGAL suggests that its effectiveness is likely due to the efficient alignment of modalities rather than relying solely on modality-specific encoding. This approach allows MADRIGAL to leverage information from various data sources more effectively, improving predictive capabilities for drug combinations.

MADRIGAL improved upon multimodal (KG-structure) models by 22.5% and 12.8% in AUROC in the two datasets on average, under this challenging split (Fig. 2b). Similar performance gains are observed across other dataset splits, demonstrating that MADRIGAL advances drug combination outcome prediction through the integration and alignment of diverse modalities (Supplementary Fig. S3). Ablation studies validated the contributions of contrastive learning and multimodal learning across both datasets compared to using only structural information, showing that MADRIGAL’s performance benefits from including multiple data types (Fig. 2b, Supplementary Fig. S3).

To evaluate the robustness of MADRIGAL, we examined its predictive precision in drug safety datasets. Our analysis hypothesizes that test drugs with greater representation and structural similarity to drugs in the training set yield a higher prediction accuracy for DDIs. We observed that increased structural similarity enhances DDI prediction accuracy, an effect seen

not only in the complete model (+modality alignment) but also in ablation models without alignment (+multimodal) and those relying on structure only (Fig. 2c). The similarity of the target profile further reinforces these predictions, highlighting the role of underlying biological mechanisms in drug safety modeling (Fig. 2d).

The multimodal approach in MADRIGAL outperforms the unimodal model across diverse outcomes, particularly when the modalities are aligned (Fig. 2e). Predictions for narrowly defined clinical outcomes, which correspond closely to specific biological pathways, are generally more accurate than those for broader phenotypes, underscoring the importance of pathway-specific knowledge (Supplementary Fig. S2b) [47]. Performance improvements are notable as additional modalities are integrated (Supplementary Fig. S2c). Attention weight analysis reveals that cell viability data contribute minimally, while transcriptomics plays a significant role despite its lower prevalence (Supplementary Fig. S2d).

MADRIGAL predicts drug safety profiles and captures transporter-mediated interactions.

To assess whether MADRIGAL can capture safety signals beyond drug combination contexts, we tested it on individual drugs by pairing each drug with itself as input. MADRIGAL predictions correlate with established safety profiles for specific outcomes, such as liver injury (Drug-Induced Liver Injury, DILIrank) [54], cardiotoxicity (Drug-Induced Cardiotoxicity, DICTrank) [55], and QT prolongation (Drug-Induced QT Prolongation Atlas, DIQTA) [56] (Fig. 3a-c, Supplementary Fig. S4). This shows the capability of MADRIGAL to identify clinical safety signals, even when applied to single drugs.

We used MADRIGAL to examine a common mechanism of DDIs—shared transport mechanisms among drugs [57, 58]. Membrane transporters play a crucial role in drug absorption, distribution, and elimination, and their shared use by multiple drugs can lead to significant DDIs. A comprehensive study by the International Transporter Consortium [59] revealed that approximately 75% of the top 200 prescribed drugs are substrates for at least one transporter, and many of these drugs interact with multiple transporters, creating a high potential for transporters to play a role in the governance of drug absorption and disposition and in mediating clinical DDI.

Transporter-mediated DDIs [57], such as doxycycline's interactions with digoxin, warfarin, tacrolimus, and levetiracetam, are effectively captured by MADRIGAL (Fig. 3d). Specifically, MADRIGAL assigned a very high normalized rank (prediction score ranked among all DrugBank drugs then normalized to [0,1], see Methods. 5.1), indicating a less favorable safety profile, to the doxycycline-tacrolimus pair and a moderately high rank to doxycycline-levetiracetam, despite neither pair being present in MADRIGAL's dataset. Drugs that share

transporters, enzymes, or carriers showed a significantly higher tendency for interaction in MADRIGAL’s predictions (Fig. 3e). For drugs that share specific transporters, which the regulatory guidelines recommend for evaluation due to organ-specific safety risks [58], MADRIGAL also highlighted transporter-related safety events (Fig. 3f). This accuracy underscores MADRIGAL’s potential as a tool for preemptively identifying risks for drug interactions early in drug development both from a clinical pharmacology perspective and in combination drug development.

MADRIGAL predicts safety profiles of oncology drug combinations.

Balancing efficacy and safety in combination cancer therapies is challenging due to the severe toxicity profiles of treatments such as chemotherapy, where safety testing often restricts which combinations progress to efficacy studies [60]. We investigate MADRIGAL for combinations that include PARPi¹, a class of targeted therapies used to treat breast and ovarian cancer [61].

We first examine whether known neutropenia and hematological effects of PARPi combinations are captured by MADRIGAL (as shown in Fig. 4a). The olaparib + paclitaxel combination, with a predicted safety rank exceeding 750, was associated with higher rates of grade 3 and 4 hematological adverse effects, such as neutropenia, in gastric cancer patients [62]. In contrast, the combination of olaparib + abiraterone, which had a predicted safety rank of 300, was studied in metastatic castration-resistant prostate cancer (mCRPC) [63]. The latter combination, administered in conjunction with prednisone or prednisolone, has been approved in the US for adult patients with deleterious or suspected deleterious BRCA-mutated mCRPC (BRCAm) [64], and in the EU for adult male patients with mCRPC in whom chemotherapy is not clinically indicated [65]. The adverse effects of drug combinations, including hematologic toxicities, can be explained by the pharmacological properties of the drugs in addition to the symptoms or etiology of the disease [66]. Hematological toxicities, such as neutropenia, are largely attributable to drug-induced myelosuppression, a common property of chemotherapy agents. These findings indicate that the safety classifications predicted by MADRIGAL capture broad hematological adverse events of drug combinations that are generalized between types of cancer and patient populations.

The combination of olaparib + paclitaxel is predicted to have a higher risk of hematological and neutropenia-related adverse events than olaparib + ceralasertib, which is a combination that is being clinically investigated with incomplete safety characterization (Fig. 4a

¹Included in the analysis were PARPi’s that are FDA-approved or in late-phase clinical trials and are sufficiently represented in the dataset (with at least five different drug combinations and data for at least two outcomes).

shows median-aggregated scores across neutropenia and hematological effects, Supplementary Fig. S5a shows mean-aggregated scores). In plasmaMATCH [67], CAPRI [68, 69], and VIOLETTTE [70] studies (up to Phase II), the combination of olaparib + ceralasertib showed a manageable safety profile, with adverse events consistent with those expected from each drug individually and no new significant safety concerns. The combination of olaparib + paclitaxel, however, evaluated in the Phase III GOLD trial [62], resulted in grade 3 or worse neutropenia adverse events in 30% of patients with advanced gastric cancer. The olaparib + abiraterone combination has received FDA approval [64], with 5% of mCRPC patients experiencing grade 3 or worse neutropenia in the Phase III PROpel trial [63].

Of note, our dataset does not include annotated outcome data for the olaparib + abiraterone and olaparib + ceralasertib combinations, while the olaparib + paclitaxel combination is only annotated with an increase in metabolic activity. The hematological annotations for olaparib in the dataset include an increased risk of bleeding, methemoglobinemia, neutropenia, and thrombocytopenia, and these effects are documented for combinations involving only 12 other drugs. Other PARP inhibitors, such as rucaparib and talazoparib, have even fewer annotations related to hematological outcomes in the dataset. Combinations of these drugs and local anesthetics are associated with an increased risk of methemoglobinemia, with no other documented hematological effects, and methemoglobinemia is a rare adverse effect associated with local anesthetics [71, 72]. In addition to the prediction of increased risk of neutropenia (0.998, 8/141) for olaparib + paclitaxel as presented above, metabolism, excretion, myelosuppression, gastrointestinal ulcers, cardiotoxicity, and liver damage are among the top 10 adverse events predicted by MADRIGAL. The prediction of liver damage aligns with the complications observed in the GOLD study. In the (olaparib + paclitaxel) treatment arm, liver damage was reported as a treatment-related adverse event and was implicated in the death of one patient [62].

Anemia is a well-documented adverse event associated with PARPi's and can be clinically managed [64]. Since the dataset of MADRIGAL does not include any associations between PARPi and anemia, this adverse effect is used as a positive control to evaluate MADRIGAL to detect effects that occur in patients, but are not included in the dataset. We prompted MADRIGAL-LLM with a description of anemia (Fig. 7f). MADRIGAL predicted significantly higher scores for anemia in olaparib + abiraterone combination compared to random drug combinations (p -value < 0.05, two-sided Mann-Whitney U).

Next, we investigate organ-specific effects of PARPi combined with other anti-cancer drugs (Methods Sec. 5.3). For each PARPi, we use MADRIGAL to make predictions for its combination with all other anti-cancer drugs we curated across hematological, renal, and hepatic

outcomes (Fig. 4b, Methods Sec. 5.3). Hematological adverse events are well-documented side effects of PARPi, both when used as monotherapies and in combination therapies [64, 73, 74]. Among these, "neutropenia, increase" is consistently ranked as a highly predicted effect for all PARPi combinations (olaparib: 7/141; talazoparib: 9/141; rucaparib: 3/141). Systematic review of hematological adverse events [75] shows minor differences between olaparib and rucaparib. Renal adverse events, such as increased blood creatinine and acute kidney injury, have been reported in the TRITON2 trial of rucaparib [74] and in eight clinical trials of olaparib [64], including the PROpel trial investigating the olaparib + abiraterone combination [63]. Four of these eight trials reported that over 25% of participants experienced an increase in serum creatinine. Although MADRIGAL's dataset does not include these specific renal events, MADRIGAL predicts high scores for renal-related adverse events across PARPi combinations, demonstrating its ability to generalize beyond the training data. These include changes in excretion (1/141 in all three PARPi's), serum levels (talazoparib: 4/141; rucaparib: 14/141), serum levels excretion rate (olaparib: 5/141; talazoparib: 6/141; rucaparib: 5/141) and serum levels of active metabolites (olaparib: 14/141; talazoparib: 17/141; rucaparib: 13/141), indicating a potential risk of renal safety events. The EMBRACA trial [76] of talazoparib in patients with advanced breast cancer and germline mutations in BRCA1/2 reported one drug-related death in the talazoparib group due to veno-occlusive liver disease. Increased aminotransferase levels were identified as common adverse reactions (occurring in more than 20% patients) in the EMBRACA trial (aspartate and alanine aminotransferases) and in the GOLD trial of olaparib combined with paclitaxel, where elevations of alanine aminotransferase were reported in more than 10% of patients [62].

The renal and hepatic effects described above are also associated with transporter inhibition, a characteristic of olaparib and rucaparib [64, 74]. Differences in predicted renal and liver outcomes for talazoparib compared to rucaparib and olaparib (aggregated scores of 0.937 vs. 0.955 and 0.947 for renal effects; 0.939 vs. 0.958 and 0.957 for liver effects, Figure 4b) align with in vitro findings indicating distinct inhibitory profiles of these PARP inhibitors on enzymes and transporters. Specifically, olaparib and rucaparib act as inhibitors and inducers of multiple enzymes and as inhibitors of various transporters [64, 74], whereas talazoparib has minimal impact on enzymes and transporters [73]. These differences raise the possibility of olaparib- and rucaparib- (but not talazoparib-) specific drug interactions with enzyme- and transporter-related mechanisms, which have also been suggested by pharmacokinetic studies [77].

Drug combinations approved or under clinical investigation have undergone a thorough safety investigation. As such, we next seek to examine whether drug combinations involving

PARPi (“PARPi combination”) that are being clinically investigated or approved are predicted by MADRIGAL as having more favorable safety profiles. PARPi combinations in which the other drug is any cancer drug are treated as a negative control. We found that those clinically investigating or approved PARPi combinations, curated from [64, 73, 78], are predicted by MADRIGAL to have a more favorable safety profile than PARPi combinations (with any other cancer drug) in endocrine, heart, kidney, and liver effects, and comparable in blood and gastrointestinal effects (Fig. 4c). In all organs except the liver, these combinations are predicted to have a more favorable safety profile compared to clinically investigated drug combinations, including those actively investigated in 2024, those that have failed clinical trials or those that have been withdrawn [79]. Drug combinations already used in patients and listed in the US FDA Orange Book are predicted to exhibit the most favorable safety profiles across all organs, with the exception of the heart, which is used as a positive control.

We visualize the normalized ranks of all outcomes for each PARPi combination currently under clinical investigation, including the (olaparib + paclitaxel) combination to serve as a reference for a combination with known safety concerns. All PARPi combinations under investigation are predicted by MADRIGAL to have a more favorable safety profile compared to the control (Fig. 4d, from left to right with increasing average of the top five highest normalized ranks). Based on this average, we observe that PARPi combinations that have progressed to advanced stages of clinical development, as well as those that are approved, are generally predicted to have more favorable safety profiles than those in earlier phases. Since early-stage trials, particularly phase I, primarily focus on assessing candidate safety, these combinations often have less well-established safety profiles compared to those in advanced phases or approved for use. The predictions made by MADRIGAL align with this trend, as the variations in safety profiles among phase I combinations suggest differences in their suitability for clinical development.

Polypharmacy management in chronic metabolic disorders using MADRIGAL.

The management of chronic metabolic disorders often involves complex polypharmacy due to comorbid diseases that require the concurrent use of multiple drugs. The incomplete mechanistic understanding of many therapies, coupled with the intricate and overlapping pathophysiology of these disorders, underscores the importance of combination therapies [80] This complexity is particularly evident in conditions such as type II diabetes (T2D) and MASH, both of which are increasingly prevalent [81, 82] and characterized by multifaceted pathophysiology [3, 83–85]. MASH is among the most frequently cooccurring diseases in patients with T2D [82], with a global prevalence that increased from 5-7%, to more than seven times higher,

37%, among people with T2D patients [86], and occurs in up to 70% of patients with T2D in specific populations analyzed [87]. Complicating the situation even more, the FDA approved the first drug, resmetirom, for MASH only in 2024 [88]. Given the pressing need for more effective treatment protocols, combination therapies are being considered for T2D and MASH. We use MADRIGAL to investigate drug combinations in three related areas: (1) combinations for T2D and heart failure (T2D + HF), a better understood comorbidity; (2) combinations for T2D and MASH (T2D + MASH), a complex and emerging area of focus; and (3) combinations for MASH alone, where treatment options are particularly limited. To support our analysis, the T2D medications are sourced from DrugCentral [89] through PrimeKG knowledge graph [90], the Orange Book of the US FDA, and supplemented with mechanism of action data from UCSF Diabetes Teaching Center [91], Mayo Clinic [92], and Cleveland Clinic [93], and DrugBank [46]. We ensure that all medications, if not approved in the US, are marketed in Europe or Japan. Due to our focus on small molecule drugs, insulin and its analogs are excluded from this analysis.

First, we seek to validate that the predicted safety profiles of drug combinations for T2D and its comorbidities align with clinical knowledge. In the case of heart failure comorbidity, consistent with clinical observations [94], combinations involving rosiglitazone with heart failure medications are predicted to have worse safety profiles in multiple effects related to myocardial infarction or stroke compared to combinations involving pioglitazone (Fig. 5a). MADRIGAL's predictions also reflect the known risks of hyperkalemia associated with renin-angiotensin-aldosterone system (RAAS) inhibitors, including aldosterone antagonists, angiotensin II receptor blockers (ARBs), angiotensin receptor-neprilysin inhibitors (ARNi's), and ACE inhibitors (ACEi's) [95], as well as the observation that SGLT2 inhibitors may reduce the risk [96]. Combinations of these drugs with sodium zirconium cyclosilicate (SZC), a drug used to treat hyperkalemia, show significantly improved safety profiles compared to other combinations, which aligns with recent clinical practice [97, 98] and trial design [99]. Candesartan, which has a known risk of hyperkalemia [100], was used as a control (Fig. 5b). For renal effects, our model predicts that combinations of T2D medications with SGLT2 inhibitors have more favorable renal safety profiles compared to combinations with diuretics, consistent with reported clinical observations [101, 102] (Supplementary Fig. S6a).

Next, we focus on (T2D + MASH) combinations in light of the unmet need for MASH therapies. We evaluate the safety profiles of all MASH drugs or candidates currently approved, under clinical investigation, or being used off-label [103], when combined with any T2D drugs that do not share the same MoA (“rational combination”, Fig. 5c,g). The complete predicted

ranks are provided in Supplementary Fig. S6b. We also calculate the normalized rank for each MASH drug or candidate in a minimax manner (Methods Sec. 5.4). MADRIGAL ranks resmetirom, the first and only FDA-approved drug for metabolic dysfunction-associated steatohepatitis (MASH) as having the second most favorable safety profile. The predicted candidate with the most favorable safety profile, elafibranor, has demonstrated a consistent safety profile in various trials, including those for primary biliary cholangitis (PBC) [104]. However, it should be noted that in the RESOLVE-IT Phase III trial (NCT02704403), elafibranor did not show a statistically significant effect on resolving MASH without worsening fibrosis, although its safety and tolerability were consistent with previous studies. This suggests that while single-drug elafibranor efficacy in MASH might be insufficient, its safety profile may still hold potential for further exploration in combination therapies for MASH. Many of the candidates predicted to have more favorable safety profiles have safety records without serious adverse effects for effective doses in clinical trials [104–106]. While the model predicts firsocostat to have relatively favorable safety profile as well, real-world evidence suggests otherwise, particularly its association with hypertriglyceridemia [107], which is not captured in MADRIGAL dataset due to a lack of relevant effects annotations, and that firsocostat itself has no annotations of any kind. We then examine the clinical trial phases of MASH drugs or candidates and observe that when combined with T2D drugs, candidates in phase I—where the primary focus is on assessing safety—tend to exhibit less favorable safety profiles compared to those in later phases (II to IV), as expected (Fig. 5d,e). Additionally, we observed that candidates with different MoAs demonstrate varying safety profiles when combined with T2D drugs (Fig. 5f), highlighting the influence of MoA on drug safety in combination therapies.

In addition to developing monotherapies for MASH, multiple trials have explored combination therapies to understand the mechanisms underlying the safety and efficacy of drug combinations. The rationales behind MASH combination therapies broadly fall into two categories [3]: (1) Two drugs target independent pathways or two components of one pathway, leading to improved efficacy through independent action or synergy [1], especially given the complexity of MASH (enhanced efficacy); (2) A drug addresses MASH, while a secondary drug mitigates the adverse effects associated with the primary therapy (enhanced safety) (Fig. 5g). We annotate drug combinations currently under clinical investigation for MASH [3,84,85,108] into these two categories. While the annotation of enhanced safety or efficacy was based on literature curation, these categories are not mutually exclusive—some combinations may confer both safety and efficacy benefits. We then ranked the safety of these combinations based on the average of the top five normalized ranks among all possible pairwise combinations of

MASH drugs or candidates within the same MoA class (“background combinations”), representing relative safety among possible alternative combinations that share similar combination rationales. We observe that 3 out of 5 combinations curated for enhanced safety and 5 out of 11 combinations curated for enhanced efficacy ranked relatively safe, which means that they were ranked first among fewer than five background combinations or ranked first or second in no fewer than five background combinations, respectively (Fig. 5h).

Predicting individualized drug combination efficacy in cancer patients with MADRIGAL.

The clinical effectiveness of cancer combination therapies can depend on the tumor genomic environment, highlighting the need to identify genomic signatures that influence therapy response [1, 60, 109]. Building on MADRIGAL’s ability to predict outcomes, we extended MADRIGAL to predict the efficacy of drug combinations in cancer patients. We adapted MADRIGAL to predict the efficacy and synergy of drug combinations in ex vivo cancer models (Fig. 6b). To validate MADRIGAL for personalized drug response predictions, we used drug response data from patient-derived xenografts (PDXE [41]) and primary cancer cells (Beat-AML [39, 40]) (Fig. 6a, Supplementary Fig. S7b). This approach can optimize combination therapies tailored to the unique needs of each patient, factoring in safety and efficacy, two key pillars of success in drug discovery and development.

In the BeatAML dataset, we sampled patients to hold out for evaluation based on gene expression profiles, somatic mutation data, and clinical information with less than 10% missing data (Methods Sec. 5.6). For each drug combination, MADRIGAL’s drug embeddings were fed into a bilinear decoder to generate a fused embedding, which was then concatenated with dimension-reduced gene expression and clinical attribute vectors before being inputted into a multi-layer perceptron. The classification target was defined as synergistic if the “combination ratio” was less than 1 [40] (Methods Sec. 1.9). Multimodal MADRIGAL combined with patient genomic profiles outperformed models without genomic input, showing the importance of patient data for strong performance (Fig. 6c). However, patient information alone was insufficient to achieve meaningful predictions without combined drug embeddings.

In the PDX dataset, we incorporated gene expression and mutation data into MADRIGAL, testing MADRIGAL’s performance by holding out each drug combination. For this dataset, we used the element-wise maximum of the two drug embeddings from MADRIGAL, concatenated with dimension-reduced gene expression data, as input to a random forest regressor. We trained two models with different regression targets: treatment response (“BestAvgResponse” [41]) and progression-free survival (PFS, “TimeToDouble” [41]). When predicting response, MADRIGAL showed statistically significant correlations between predicted and ac-

tual responses for 8 of 11 held-out drug combinations (p -value < 0.05, Kendall's τ), with an average correlation of $\tau = 0.466$ (Fig. 6d).

We stratified patients into two response categories based on predicted response using the mRECIST criterion [41]: patients with a predicted response below -20 were classified as responders and others as non-responders. For drug combinations with sufficient predicted patient responders and non-responders (≥ 5), Kaplan-Meier survival estimates showed statistically significant differences between these subgroups based on ground truth PFS (Fig. 6e,f, Supplementary Fig. S7c). When predicting PFS, MADRIGAL showed a significant correlation with outcomes for 7 of 11 drug combinations in the dataset (p -value < 0.05, Kendall's τ), with an average correlation of 0.489 (Supplementary Fig. S7d). Using the same response-based stratification approach, we confirmed that the PFS predictions aligned with the observed patient response outcome, further validating MADRIGAL's performance (Fig. 6g,h, Supplementary Fig. S7e). MADRIGAL integrates tumor genomic profiles to predict the outcomes of anti-cancer drug combinations. Using these profiles, MADRIGAL identifies patients who are more likely to benefit from specific combination therapies, allowing a more personalized approach to cancer treatment.

Enhancing MADRIGAL with an LLM for new drug combination descriptions.

We integrated MADRIGAL with a text-based LLM to address drug combination effects and outcomes beyond those encountered in MADRIGAL's training data or codified in existing medical vocabularies. Existing models are limited to controlled vocabularies, restricting their ability to predict a wider range of outcomes, highlighting the need for a flexible model that maintains predictive precision in diverse outcomes [110]. LLM-only predictors use drug names [111,112] in input prompts, which limits their ability to be used with new compounds in development that lack designated names assigned post-approval [113,114] or compounds with limited information in literature and thus poor representation in LLM's knowledge base [115].

To address this, we designed a modeling approach that combines MADRIGAL with an LLM, resulting in MADRIGAL-LLM. This model leverages text descriptions of drug outcomes from DrugBank alongside drug embeddings from contrastive pretrained MADRIGAL (without finetuning on drug combination datasets) as input to predict the likelihood of a drug pair linked to a specific outcome (Fig. 7a). Using a text-based LLM, these descriptions are converted into outcome embeddings. Placeholder tokens replace drug names in these text inputs, ensuring the LLM does not rely on specific drug names or leak information from its internal knowledge base based on drug names mentioned in the user prompt [115]. To test MADRIGAL-LLM's generalizability, we held out outcomes so that those in the test set were not encountered by

MADRIGAL-LLM during training. To further enrich the diversity of text input, we used GPT-4 to generate augmented descriptions from the perspectives of experts in medicine, pharmacology, and toxicology (Fig. 7b). This strategy exposed MADRIGAL-LLM to a spectrum of text variations in outcomes. During training, one of the ten possible descriptions (the original plus nine expert-augmented descriptions) was randomly sampled for each drug combination, allowing the model to learn from various linguistic inputs at each training step. Performance is assessed across all text descriptions for each test outcome. We included a reference score, the likelihood-weighted prior (Methods Sec. 4), which estimates the probability of a drug combination outcome in the test set based on its occurrence in the training set, adjusted for semantic similarity to known outcomes.

We evaluated whether augmented text descriptions can enhance MADRIGAL-LLM performance trained solely on original (non-augmented) outcome descriptions. Across outcomes (13/16), models trained with augmented descriptions performed better than those trained without augmentation (Fig. 7c, with three random initializations for each model). Both models trained on original and augmented descriptions performed better than baseline in most outcomes (10/16 and 12/16, respectively). We further tested MADRIGAL-LLM trained on augmented text against the original and paraphrased descriptions in the test set (Fig. 7d). In most outcomes (13/16), at least one expert-generated description improved performance over the original description, indicating the added value of expert-driven text diversity. Finally, we analyzed MADRIGAL-LLM’s predictions by measuring concordance between MADRIGAL-LLM and MADRIGAL. Using Spearman’s rank correlation, we compared predicted scores from both models for outcomes unseen by MADRIGAL-LLM (Fig. 7e, showing only correlations with p -value < 0.05 due to limited sample size in some outcomes). For most outcomes, strong positive correlations are observed, indicating that MADRIGAL-LLM effectively captures outcome patterns similar to those learned by MADRIGAL, even without explicit training on those drug combination outcomes.

Discussion

Combination therapies are essential for treating complex diseases such as hypertension, cancer, and infectious diseases, but current models often fail to translate preclinical data to predict clinical drug combination outcomes due to their focus on limited types of preclinical data, such as structural or target information. These approaches struggle to capture biological interactions that arise from multi-drug regimens. Integrating diverse data modalities, including structural data, pathways, cell viability, and transcriptomics, addresses this gap, offering a

more holistic approach to predicting drug interactions. We developed MADRIGAL, a universal multimodal model that predicts the effects of drug combinations in 953 clinical outcomes and 21,842 compounds, including approved drugs and those in development. MADRIGAL surpasses existing single-modality models and state-of-the-art techniques to predict adverse drug interactions. MADRIGAL predicts clinical transporter-mediated DDIs and safety of PARPi anti-cancer combinations and chronic conditions such as T2D and MASH. MADRIGAL also extends to personalized cancer therapies by predicting individualized drug combination outcomes from BeatAML genomic profiles and patient-derived xenograft models.

MADRIGAL can be used for preclinical predictions. When predicting adverse event risks of drug combinations to be tested in the ComboMATCH trial [60], MADRIGAL predicts elevated risk for eight combinations (Supplementary Fig. S8c). We observe correlations between proteomic changes following drug perturbations [116] and drug-drug interactions, reflecting broader pathway effects (Supplementary Fig. S8a, p -value < 0.001 between neighboring groups, Mann-Whitney U). Proteomic changes can partially explain the similarities between drug embeddings generated by MADRIGAL, even when controlling for similarities in the target profile, suggesting that MADRIGAL captures off-target and pathway effects (Supplementary Fig. S8b).

Multimodal models such as MADRIGAL can help select candidates for combination testing and offer new insights into the biological mechanisms underlying drug synergies. Flexibility in modeling outcomes and encoding drugs is crucial for the broader applicability of safety screening pipelines. By integrating MADRIGAL with an LLM, users can describe and predict clinical effects in natural language, including those not captured by existing controlled vocabularies or standardized terminologies. This flexibility helps mitigate some limitations in drug combination effects data, such as incomplete annotations for specific outcomes (e.g., neutropenia for (olaparib + paclitaxel)) that, while reported in patients [117, 118], are not yet captured in drug effect training datasets. Data biases arising from clinical practice can influence predictions, for example, when specific drugs, such as SGLT2 inhibitors, are preferentially prescribed to specific populations, such as type II diabetic patients with heart failure [119]. This could have led to different groups of drug combinations being taken by different populations with distinct underlying risks of certain adverse events. The ability to input flexible, free-form descriptions in MADRIGAL-LLM could help address these gaps by enabling scientists to benchmark candidate drug combinations, potentially increasing both the success rate in drug development and the number of patients who tolerate these combinations.

One limitation of MADRIGAL lies in the indication-agnostic nature of its training data

and predictions. Although the model is trained on datasets with coverage of drug combinations and outcomes across diverse clinically investigated and approved drugs, these datasets can lack specificity with respect to therapeutic indications, patient populations, and clinical contexts. As a result, MADRIGAL ’s safety predictions are broadly applicable but may not align with the nuanced differences across specific indications, nor fully capture clinically relevant concerns. For example, the MASH candidate firsocostat is a substrate of OATP1B1/1B3, which are transporters known to decline in patients with cirrhosis [120]. This decline could lead to differing adverse effects when firsocostat is combined with another potent OATP1B1/1B3 substrate, especially in patients at various stages of cirrhosis. This limitation positions MADRIGAL as a tool best suited for broad safety screening across diverse drug combinations rather than definitive, indication-specific safety evaluations. Nevertheless, MADRIGAL allows experts to craft queries for more focused comparisons. For example, a user could compare a new drug combination with a benchmark therapy with a known safety profile, tailored to a target population or indication. By framing such ”apples-to-apples” questions, the model can predict the relative safety of the new combination in terms of specific adverse event types. Future work could enhance this capability by integrating indication-specific information and further refining predictions for specific therapeutic contexts. In addition, factors such as the severity of the disease and prior lines of therapy should be considered.

Another limitation of MADRIGAL is that drug doses are not explicitly considered, which means that safety predictions are tied to the approved doses for each drug since these are the doses represented in FAERs and clinical databases with drug label information. Another fruitful avenue of future work includes incorporating clinical patient data to contextualize clinical safety models, as shown in our analysis, which incorporates patient genomic profiles. Drug administration practices, such as variable dosing schedules, drug administration sequence, and drug holidays, can be modeled to better reflect clinical practice, as personalized dosage adjustments have been linked to improved safety in clinical trials [121]. Predictions may be less reliable when a drug class is underrepresented in the training distribution, even if substantial preclinical data exist for an individual drug. For example, although adavosertib has cell viability and transcriptomic perturbation data, it is the only WEE1 inhibitor in the dataset. As a result, the model does not encounter similar perturbation patterns during training, leading to predictions that may not fully capture class-specific mechanisms, such as hematological adverse events associated with WEE1 inhibition [70, 122]. To address this, foundation models with knowledge-grounded retrieval [123, 124] that integrate preclinical literature can improve the representation of drug classes during model training.

MADRIGAL integrates translational pharmacology with multimodal AI to predict drug combination outcomes. It identifies interactions between approved and investigational drugs, guiding co-administration to mitigate risks. In oncology and metabolic disorders, MADRIGAL links molecular toxicity signatures to clinical outcomes, improving precision in combination therapy selection. MADRIGAL paves the way for more precise drug combination design, enhancing safety assessment and therapy selection in preclinical studies and clinical research.

Acknowledgements. We obtained the latest BeatAML dataset from Jeffrey Tyner, and we thank Christopher Eide for his help with data processing. We thank Man Qing Liang and Xiang Zhang for their helpful discussions on the TWOSIDES dataset and Payal Chandak for discussions on the PrimeKG knowledge graph. We thank Philip Isola, Shanghua Gao, Huan He, Wenxian Shi, and Michelle M. Li for their feedback on model development. We thank Ruth Johnson for her feedback on the paper and for discussions on using MADRIGAL for personalized clinical outcome prediction. We also appreciate Intae Moon’s and Walker Rickord’s comments on the manuscript. We thank Nigel Greene, Hebatallah Mohamed, and Michaël Ughetto for helpful feedback on MADRIGAL and analyses. We thank Jane Knöchel for interpreting model predictions in MASH. We also thank Diansong Zhou and Karthick Vishwanathan for their valuable insights into the analysis of cancer drug combinations. We gratefully acknowledge the support of NIH R01-HD108794, NSF CAREER 2339524, US DoD FA8702-15-D-0001, Harvard Data Science Initiative, Amazon Faculty Research, Google Research Scholar Program, AstraZeneca Research, Roche Alliance with Distinguished Scientists, Sanofi iDEA-iTECH, Pfizer Research, Gates Foundation (INV-079038), Chan Zuckerberg Initiative, John and Virginia Kaneb Fellowship at Harvard Medical School, Biswas Computational Biology Initiative in partnership with the Milken Institute, Harvard Medical School Dean’s Innovation Fund for the Use of Artificial Intelligence, and Kempner Institute for the Study of Natural and Artificial Intelligence at Harvard University. Any opinions, findings, conclusions or recommendations expressed in this material are those of the authors and do not necessarily reflect the views of the funders.

Data availability. Data and results of our analyses are shared via the project website at <https://zitniklab.hms.harvard.edu/projects/Madrigal>. Datasets are also available at Harvard Dataverse repository at <https://doi.org/10.7910/DVN/ZFTW3J>.

Code availability. Python implementation of MADRIGAL is available via the project website at <https://zitniklab.hms.harvard.edu/projects/Madrigal>. The code to reproduce results with examples of usage is at <https://github.com/mims-harvard/Madrigal>.

Authors contributions. Y.H. developed and implemented MADRIGAL, and designed evaluation setup. V.U. implemented first-stage pretraining of MADRIGAL for three modalities and integrated MADRIGAL with a large language model. Y.H. performed detailed analyses of MADRIGAL’s algorithm. X.S., V.U., and Y.H. implemented alternative methods for benchmarking. Y.H. retrieved and processed multimodal drug datasets used to train MADRIGAL models and prepared datasets for model evaluation, including the BeatAML, PDXE, cancer

combination therapies, and MASH combination therapies. N.H. retrieved and processed cell viability data used to train MADRIGAL models. Y.H., X.S., and I.L. performed analyses on cancer combination therapies. I.L. processed datasets on T2D and cancer combination therapies, and Y.H. and I.L. performed analyses on polypharmacy management. L.C., D.O., B.J., and M.G. provided expertise on clinical pharmacology and safety of drug combinations. M.Z. designed and led the study. All authors contributed to writing the manuscript.

Competing interests. L.C., D.O., and M.G. employees and stockholders of AstraZeneca. B.J. performed this research while he was employed by AstraZeneca. The remaining authors declare no competing interests.

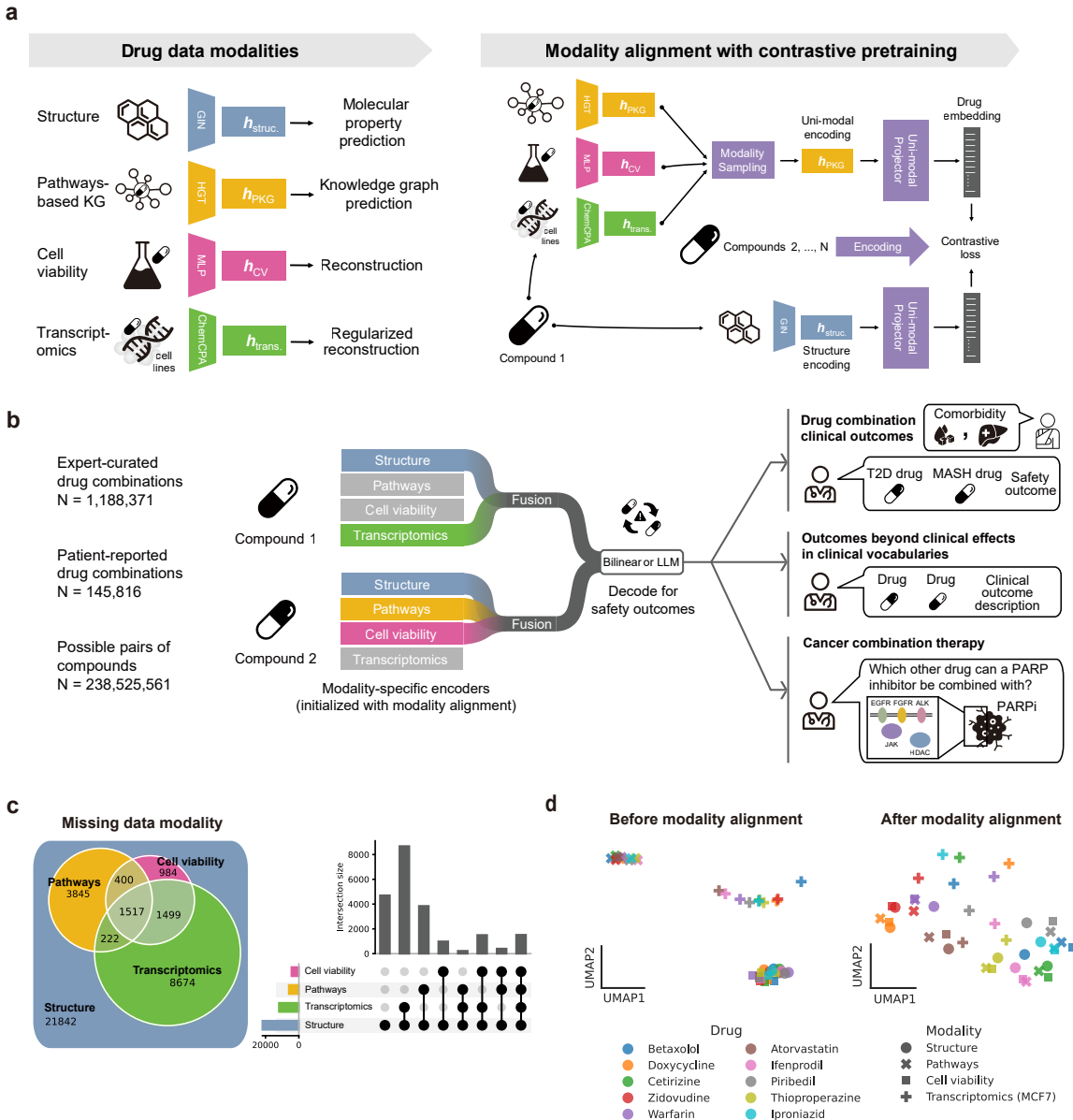


Figure 1: MADRIGAL integrates multimodal preclinical data to predict clinical outcomes of drug combinations. **a**, Overview of data modalities and the modality alignment framework. The modality-specific encoders are aligned via contrastive pretraining. MADRIGAL extracts information from multimodal data using specialized encoders (Methods Sec. 2). **b**, Comprising modality-specific encoders, a fusion module, and a decoder, MADRIGAL is trained on expert-curated and patient-reported drug combination datasets to predict safety and efficacy outcomes. A customized transformer encoder with bottleneck tokens enhances fusion (Methods and Supplementary Fig. S1). The model enables three key applications: prediction of safety outcomes in patients receiving multiple medications, rational design of combination therapies in oncology by modeling interactions between targeted therapies and other anticancer agents, and flexible outcome description by incorporating diverse biomedical signals beyond predefined ontologies. **c**, The missing data modality problem is evident in the scarcity of drugs with more than two available modalities, motivating our three-stage optimization procedure, including a modality alignment step. We treat cell lines in transcriptomics as separate modalities in the fusion module (Supplementary Fig. S1), throughout the text and illustrations, we will refer to transcriptomics as a single modality to enhance readability and clarity. This distinction is intended to be self-evident from context. **d**, Illustration of modality-specific latent representations of ten randomly sampled drugs, shown before and after modality alignment in MADRIGAL. Prior to alignment, representations cluster by data type, while post-alignment, they reorganize based on drug identity, enabling cross-modal integration.

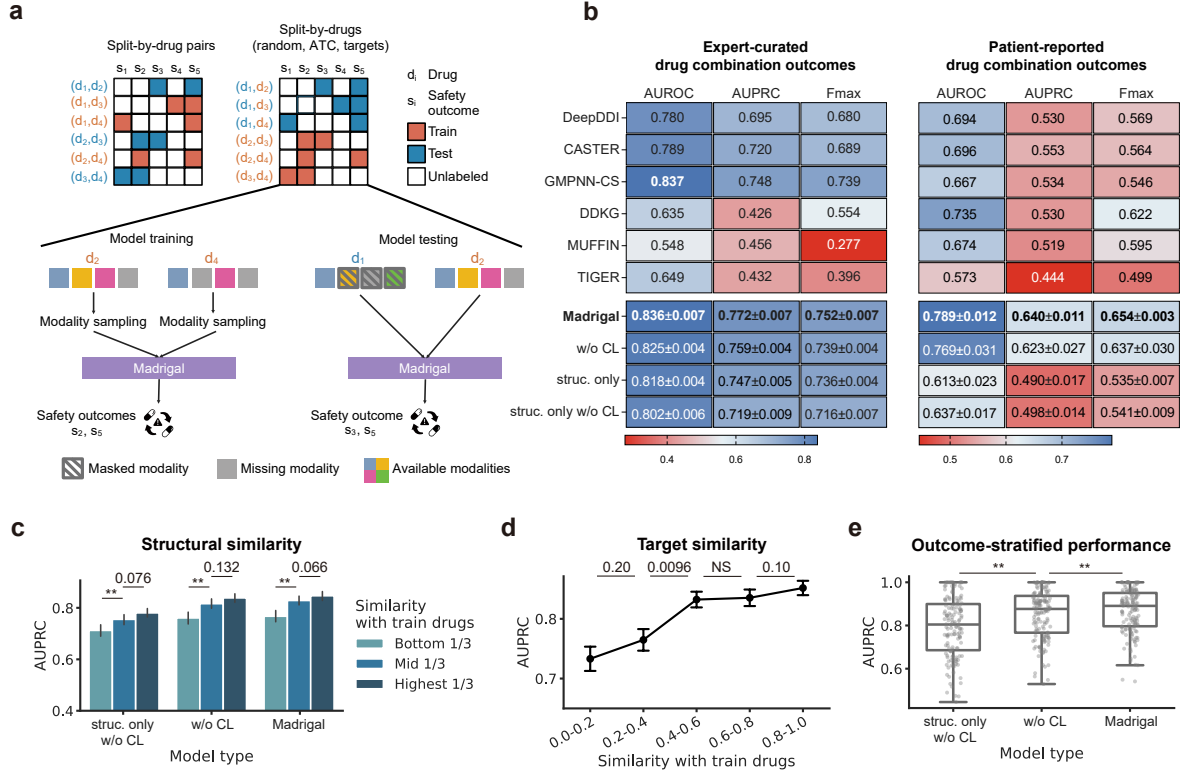


Figure 2: Benchmarking MADRIGAL and performance analyses. **a**, Data splitting strategy for predicting safety outcomes of drug combinations. The split-by-drug pairs and split-by-drugs setups are illustrated for four drugs d_1, d_2, d_3 , and d_4 with varying modality availability, and five outcomes s_1, s_2, s_3, s_4 , and s_5 . In the split-by-drugs setup, we display the training and evaluation setups. During training, all available modalities are used (for d_2, d_3, d_4); however, at testing, other modalities are masked (patterned boxes) for test drugs (d_1), allowing only the structure modality to be available. **b**, Test performance of MADRIGAL in the DrugBank (expert-curated drug combination outcomes) and TWO SIDES (patient-reported drug combination outcomes) datasets. In the split-by-drugs (target) dataset split, test drugs are chosen such that they have minimal overlap in their target profile with the train drugs (Methods). “w/o CL” refers to the ablation model without modality alignment; “struc. only” refers to the ablation model with only structure modality during finetuning (but with all modalities during modality alignment); and “struc. only w/o CL” refers to the ablation model without modality alignment and with only structure modality available during finetuning. AUROC: area under the receiver operating characteristic curve; AUPRC: area under the precision-recall curve; Fmax: maximum of F-measure. **c,d**, Test performances increase for test drugs of increasing similarity levels to train drugs in terms of structure (c) and target profile (d). The progression from “struc. only w/o CL”, “w/o CL”, to MADRIGAL represents progressive additions of multimodal input and modality alignment upon a simple model only taking molecular structure input. For each test drug, its structural similarity (with the train set) is calculated as the average of the highest 5 Tanimoto similarities between its Morgan Fingerprint with any train drug’s fingerprint. Target profile similarity is similarly defined as the average of the highest 5 Jaccard similarities between the drug’s target profile with any train drug’s profile. Target profiles of drugs are set of targets annotated to the drugs, obtained from DrugBank [46]. Errorbars show 95% confidence interval. Two-sided Mann-Whitney U test; ** p -value < 0.005 . **e**, Test performance of MADRIGAL ablation with only structure modality, ablation without modality alignment (but with multi-modality), and full model, stratified by safety outcomes. Analyses in (c-e) are performed with models trained on the DrugBank dataset, split-by-drugs (random) setting. Two-sided Wilcoxon signed rank test; ** p -value < 0.005 .

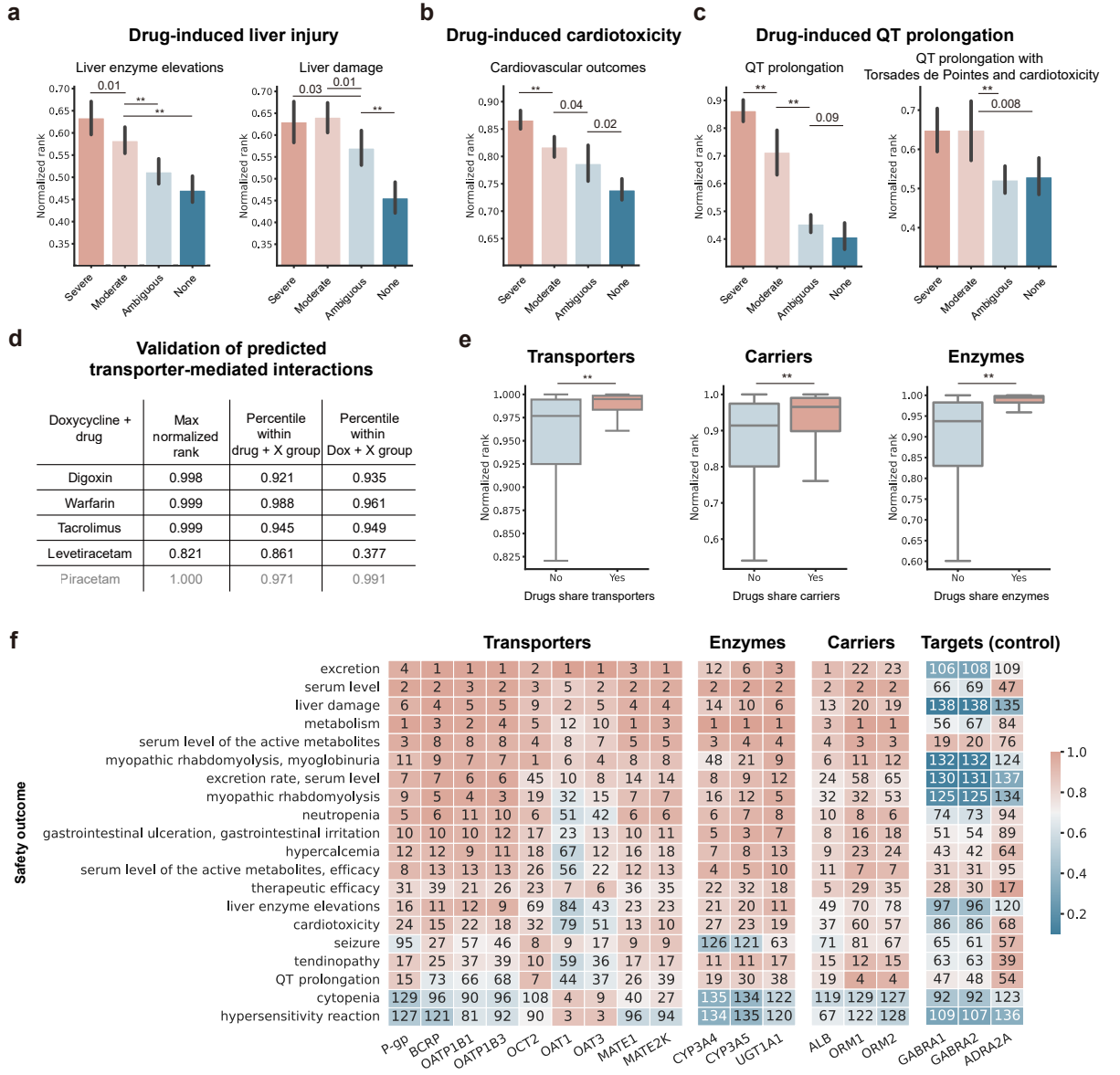


Figure 3: Evaluating MADRIGAL predictions on external patient safety datasets. **a-c**, Model predictions of individual drug's organ-specific adverse effects correlate well with concern levels in three organ-specific adverse effect datasets (drug-induced liver injury, drug-induced cardiotoxicity, drug-induced QT prolongation). Predictions of adverse effects of individual drugs are produced by duplicating the same drug as a drug pair to input to the model, and the normalized rank of each drug is then generated by ranking all such duplicate drug pairs according to their predicted scores. Error bars show 95% confidence interval. Two-sided Mann-Whitney U test; ** p -value < 0.005 . By default, samples in neighboring concern levels are tested. No connecting lines between neighboring concern levels indicates NS. **d**, Model predictions of potential transporter-mediated DDIs (Methods Sec. 5.2) correlate with newly-reported transporter-mediated DDIs [57], involving doxycycline (Dox) plus multiple other drugs. Piracetam is included as a reference as it is structurally highly similar to levetiracetam. For each drug pair, the max normalized rank is the maximal normalized rank among all potential transporter-mediated DDIs among safety outcomes from DrugBank. Percentiles compare the max normalized rank of Dox + X among either X + any curated DrugBank drug ("drug + X group") or Dox + any curated DrugBank drug ("Dox + X group"). **e**, Drugs sharing the same transporters, carriers, or enzymes are predicted to have a higher tendency to have relevant safety outcomes (Methods Sec. 5.2). Transporter, carrier, and enzyme information of drugs are obtained from DrugBank [46]. The highest normalized rank among all potential transporter-, carrier-, or enzyme-mediated safety outcomes is considered for each drug pair (see Methods Sec. 5.2). Two-sided Mann-Whitney U test; ** p -value < 0.005 . **f**, Drugs sharing specific transporters are predicted to have a higher tendency of both common and specific transporter-related safety outcomes. Transporters recommended by regulatory authorities to examine organ-specific safety outcomes are taken from [58]. Safety outcomes shown are ranked in the highest 10 for at least one transporter (across all drug pairs sharing it). The color of each cell reflects the aggregated normalized rank (median across all drug pairs sharing corresponding transporter), and the number in each cell is the ranking (max=158) of the aggregated normalized rank of the corresponding safety outcome among all safety outcomes for drug pairs sharing the corresponding transporter. The safety profiles of drugs sharing three enzymes, carriers, and targets, respectively, are also shown for comparison.

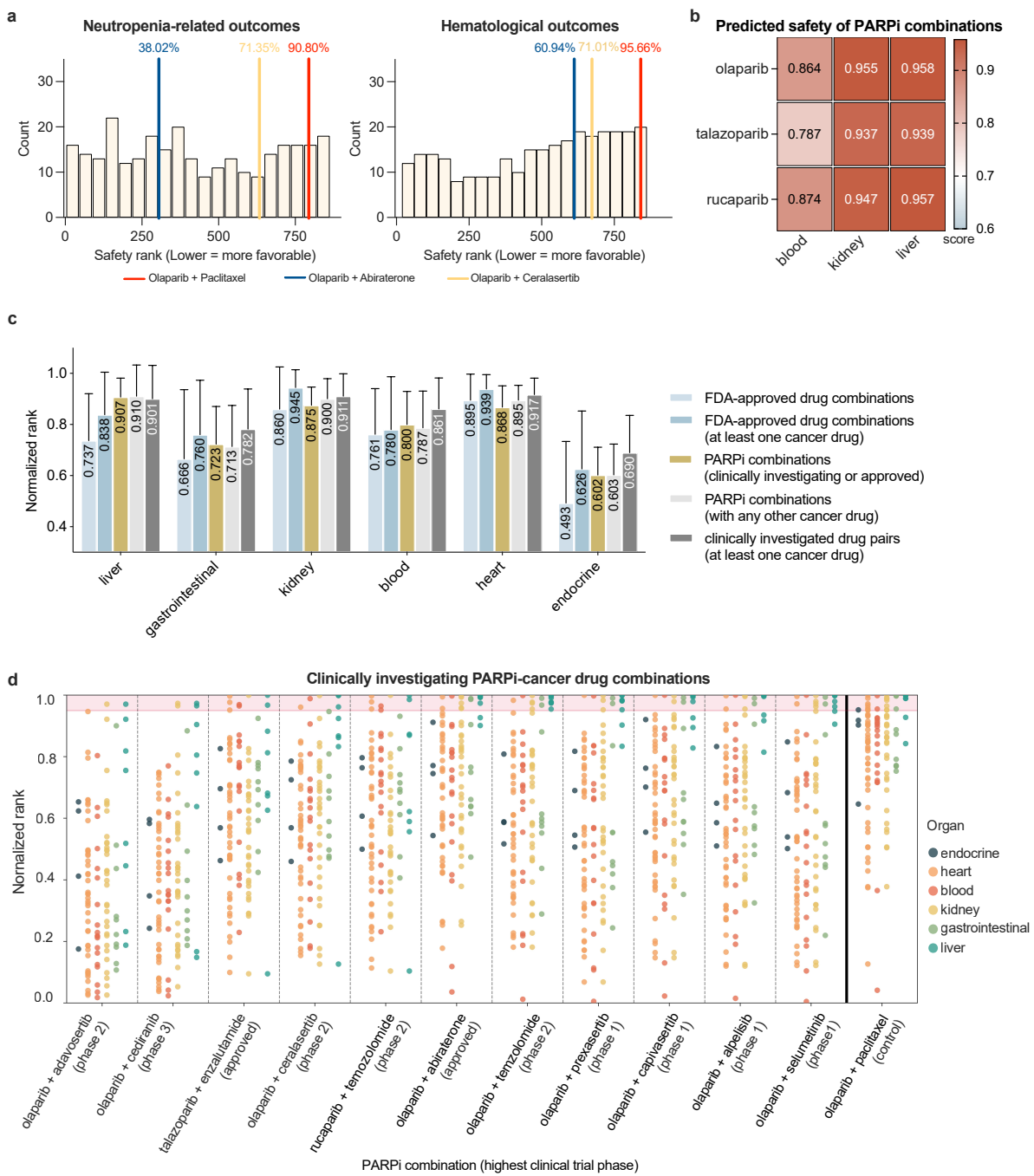


Figure 4: (Caption on the following page.)

Figure 4. MADRIGAL retrieves and ranks drug combinations based on predicted safety profiles for cancer therapy. **a**, Distribution of predicted hematological safety risks for clinically established PARP inhibitor (PARPi) combinations. The figure compares the safety ranks of an approved combination with an acceptable safety profile (olaparib + abiraterone), a combination associated with unacceptable dose-limiting toxicities (olaparib + paclitaxel), and an investigational combination with incomplete clinical safety characterization (olaparib + cerasertib). The normalized rank of each combination for a given safety outcome is derived by ranking the predicted probability of the outcome relative to all pairwise drug combinations. The ranking score is computed as the median normalized rank across neutropenia-related adverse outcomes (“neutropenia, increase”, “cytopenia, increase”, “myelosuppression, anemia”, “severe leukopenia, increase”, and “neutropenia, thrombocytopenia, increase”), or all hematological toxicities. The safety rank of each combination is then derived by ranking the score relative to all pairwise combinations of PARPi with another oncology agent (Methods Sec. 5.3), where a numerically lower rank indicates a more favorable safety profile. **b**, Predicted organ-specific toxicity profiles of PARPi-containing combinations. Organ-specific safety scores for each PARPi-drug pair (holding a PARPi fixed while varying the paired drug) are computed as the average of the three highest predicted normalized ranks for the organ system. The median of these scores across all tested drug combinations involving a specific PARPi summarizes its predicted safety profile across different organ systems. **c**, Comparative safety assessment across different classes of drug combinations. Left to right bars within each group represent: (1) FDA-approved drug combinations, (2) FDA-approved combinations where at least one drug is an oncology agent, (3) clinically investigated or approved PARPi combinations, (4) all tested pairwise combinations of a PARPi with another oncology agent, and (5) clinically investigated drug combinations where at least one drug is an oncology agent. Each drug combination’s safety profile is represented by the average of the five highest normalized toxicity outcome ranks for each organ system. Higher ranks indicate greater predicted safety concerns. **d**, Predicted safety profiles of PARPi-containing drug combinations undergoing clinical investigation or approved for clinical use. Drug combinations are ranked in ascending order based on the average of the five highest normalized toxicity outcome ranks. The (olaparib + paclitaxel) combination, which has been associated with significant hematological toxicities in clinical trials, serves as a reference for a combination with known safety concerns.

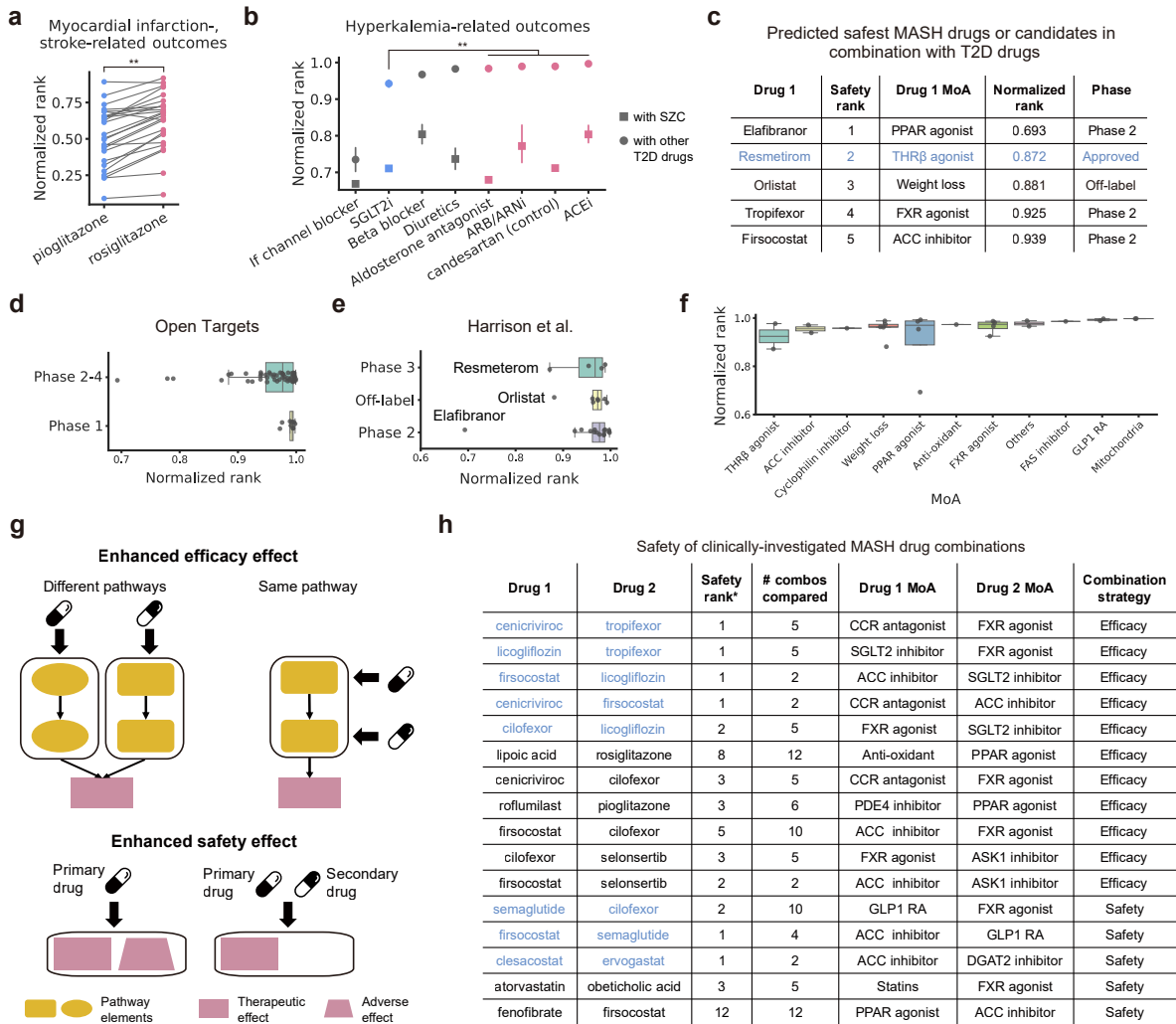


Figure 5: MADRIGAL evaluates drug combinations for metabolic disorders, including type II diabetes (T2D) and metabolic dysfunction-associated steatohepatitis (MASH). a, Predicted safety profiles of drug combination involving pioglitazone or rosiglitazone with heart failure medicine correlate with clinical concerns of myocardial infarction- and stroke-related safety outcomes (see Methods Sec. 5.4). Each point represents the median of normalized ranks of pioglitazone or rosiglitazone, when combined with any drug indicated for heart failure, with regard to each relevant safety outcome. Blue and red indicate the clinically perceived safety of respective drugs, with blue being safer and red being more unsafe. Two-sided Wilcoxon signed rank test; ** p -value < 0.005. b, Predicted safety profiles of drug combination involving one heart failure medicine and another T2D drug correlate with clinical concerns on hyperkalemia. For each combination involving a heart failure medicine and a T2D drug that does not share the same MoA, the max of normalized ranks with regard to hyperkalemia-related safety outcomes are taken (“hyperkalemia, increase”, “hypotension, hyperkalemia, nephrotoxicity, increase”, “renal failure, hyperkalemia, hypertension, increase”, and “renal failure, hypotension, hyperkalemia, increase”). Heart failure medications are then grouped based on their MoA. Blue and red colors indicate the perceived safety of respective drugs, with blue being considered to be less associated with hyperkalemia, gray being no direct evidence, and red being considered to be more associated with hyperkalemia. SGLT2i, sodium/glucose cotransporter 2 inhibitor; ARB, angiotensin II receptor blocker; ANRi, angiotensin receptor/neprilysin inhibitor; ACEi, angiotensin-converting enzyme inhibitor; SZC, sodium zirconium cyclosilicate; HF, heart failure. Error bars show 95% confidence interval. Two-sided Mann-Whitney U test; ** p -value < 0.005. c, Predicted safety of MASH clinical candidates from [103] in combination with T2D drugs (only shown predicted safest 5 candidates). Drug 1 stands for MASH drugs or candidates, and the drug 2 (not shown) here are all T2D drugs or candidates, similar as in (b) (Methods Sec. 5.4). Safety rank is derived by ranking the normalized ranks shown on the right. The blue row highlights resmetirom, the first FDA-approved drug for MASH, which happened in 2024. PPAR, peroxisome proliferator-activated receptor; THR β , thyroid hormone receptor beta; FXR, farnesoid X receptor; ACC, acetyl-CoA carboxylase. d, Predicted safety profiles of MASH clinical candidates in different clinical trial phases (from Open Targets [125], EFO:0003095), when used in combination with T2D drugs. The score of each MASH clinical candidate is computed in a “minimax” manner, where we first take the average of the highest 5 normalized ranks across all outcomes for each drug combination, then take the average of the lowest 5 such averages for each MASH clinical candidate (i.e. considering 5 safest T2D drugs to be combined with). e, Predicted safety profiles of combining MASH clinical candidates in different clinical trial phases (from [103], as of its publication date) with T2D drugs. Scores are calculated similarly as in (d). f, Safety profiles when combining MASH clinical candidates (same as in c) with T2D drugs. Scores are calculated similarly as in (d). g, Example efficacy and safety rationales for developing combination therapies. h, Predicted safety profiles of clinically investigating combination therapies for MASH. Blue rows highlight those drug pairs that are predicted to be relatively safe among its “rational background” of all pairwise combinations between the two drugs’ respective mechanism of action categories (defined in Main). *: Safety ranks among the “rational background” of drug combinations.

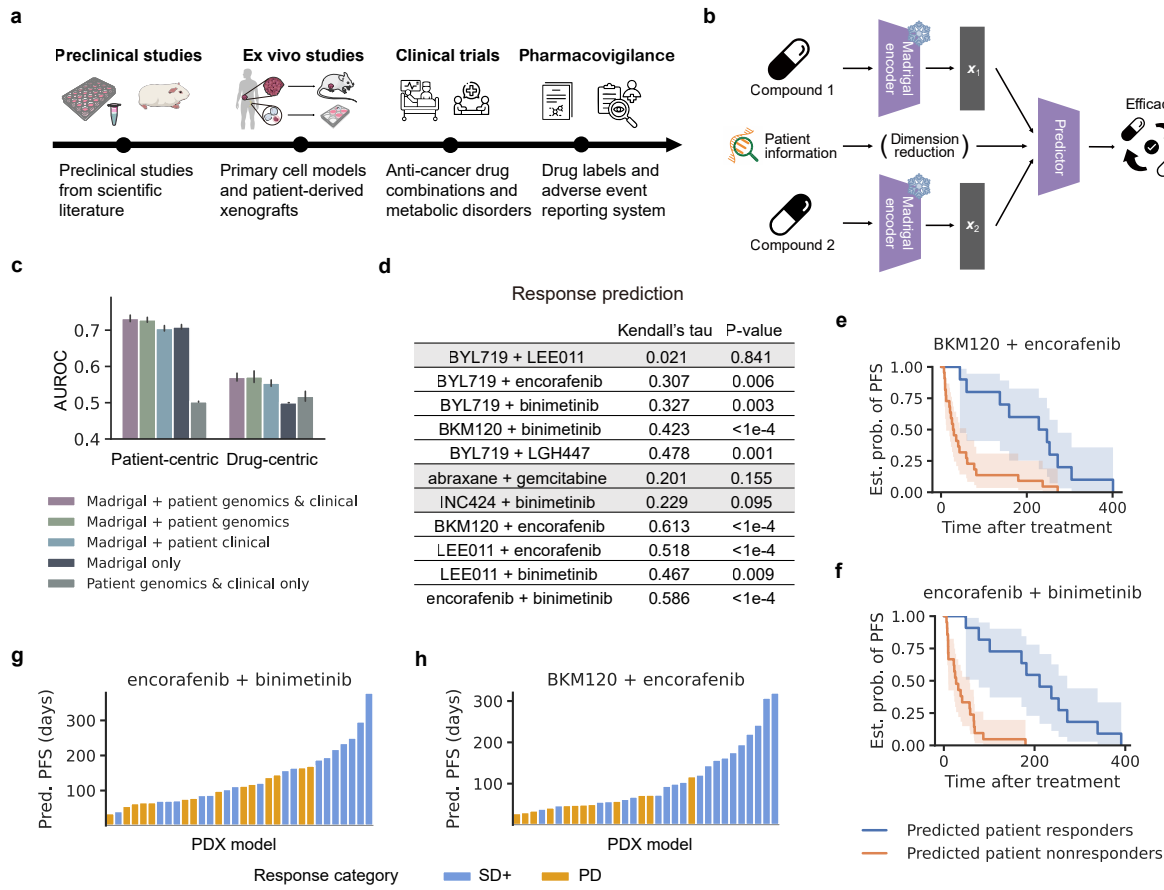


Figure 6: MADRIGAL predicts effective drug combinations tailored to individual patients. **a**, Drug combination datasets to which MADRIGAL is applied, spanning multiple stages of the drug development pipeline, including preclinical studies, ex vivo studies, clinical trials, and post-marketing surveillance. **b**, Predicting personalized drug combination efficacy using MADRIGAL’s encoder. The encoder parameters are frozen, and drug encodings, along with dimension-reduced patient-specific features (genomic and/or clinical attributes), are input into a predictor module to generate efficacy predictions. **c**, Performance of MADRIGAL in predicting synergistic drug combinations in BeatAML [39], where prediction target is combination synergy (Methods Sec. 5.6). Model evaluation is conducted on randomly held-out patients. Patient-centric and drug-centric denote two ways of calculating AUROC to evaluate the model (Methods Sec. 5.6). Error bars show 95% confidence interval. **d**, Performance of MADRIGAL in predicting drug combination efficacy in PDX Encyclopedia [41] under a leave-one-drug-combination-out setup. The prediction target is treatment response (BestAvgResponse), and the evaluation metric is Kendall’s tau correlation. **e**, Kaplan-Meier survival estimates stratified by predicted treatment response for the (BKM120 + encorafenib) combination. The predictor is trained on other drug combinations, with treatment response as the prediction target (same predictor as in (d)). Two-sided log-rank test; p -value = 0.001. **f**, Same as (e) but for the (encorafenib + binimetinib) combination. Two-sided log-rank test; p -value < 1e-4. **g**, Predicted progression-free survival (PFS, TimeToDouble) for individual patient models treated with the (encorafenib + binimetinib) combination. The predictor is trained on other drug combinations, with PFS as the prediction target. Predictions are color-coded by the observed best response category (calculated from response according to mRECIST [41]) of each patient model, SD+ = stable disease or partial response or complete response, PD = progressive disease. **h**, Same as (g) but for the (BKM120 + encorafenib) combination.

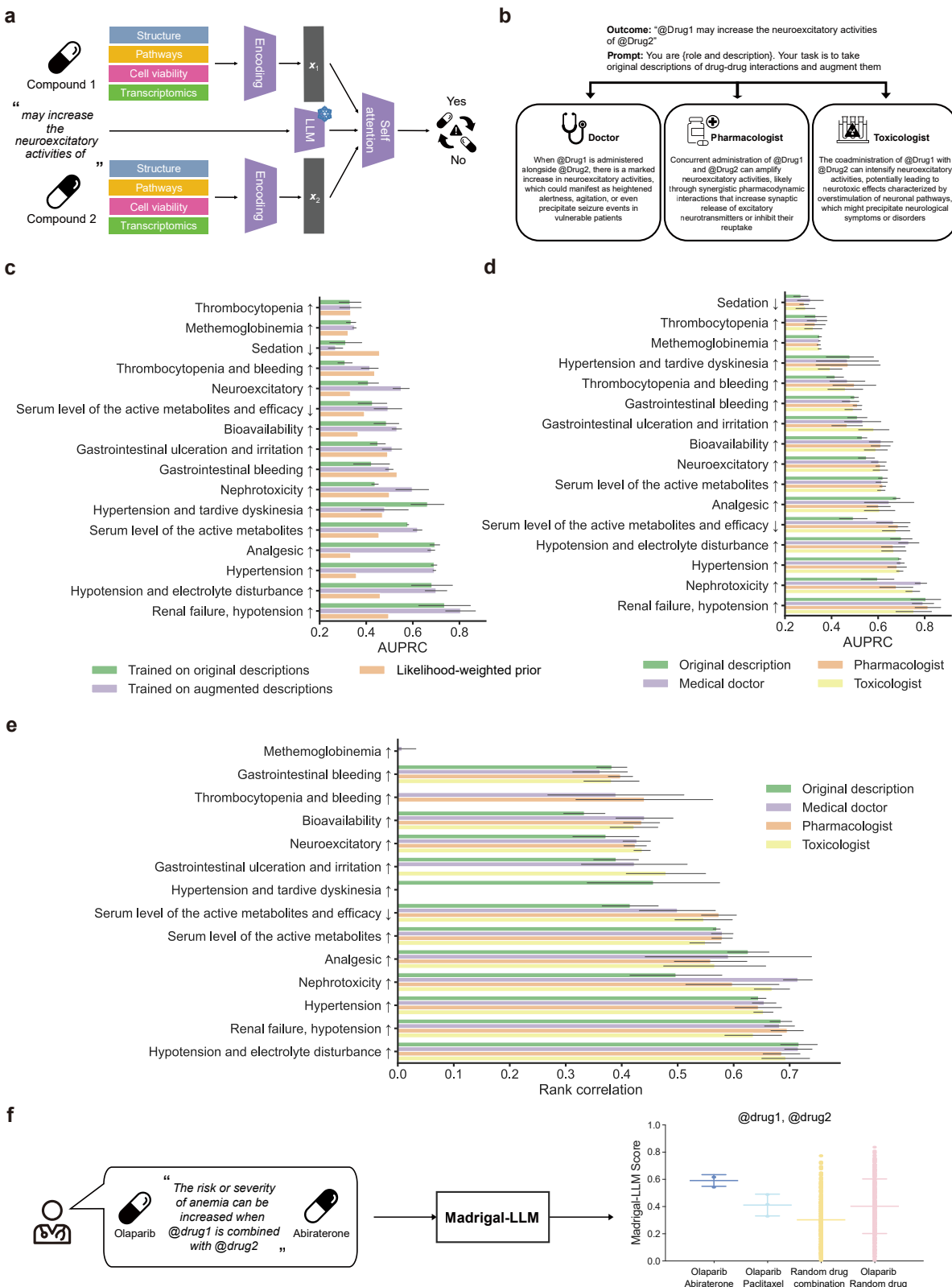


Figure 7: Flexible descriptions of safety outcomes through a LLM decoding module. **a**, The MADRIGAL-LLM architecture involves processing the two drugs with modality-specific encoders and the fusion module as MADRIGAL, plus a pre-trained LLM (Mistral-7B [126]) to obtain encodings for free-text descriptions of safety outcomes. The parameters of the LLM are frozen. The encodings of the drugs and the free-text descriptions are fed into a trainable self-attention layer, and a trainable MLP layer is then applied to concatenated encodings to obtain the final prediction for the safety outcome described in free text. **b**, Free-text descriptions of safety outcomes are augmented using GPT-4 to obtain more diverse and potentially informative descriptions. We construct a proper prompt and query GPT-4 to generate augmentations as if it were an expert Doctor, Pharmacologist, or Toxicologist (Methods Sec. 4.1). **c**, Test performance of MADRIGAL-LLM is shown across unseen safety outcomes for the cases where the model is trained on only the original text descriptions and where it is trained on augmented descriptions. Only original text descriptions of unseen safety outcomes are used to evaluate performance in both cases to ensure a fair comparison. **d**, Test performance of MADRIGAL-LLM trained with augmented descriptions across unseen safety outcomes, with different text description types (original and augmented) used for evaluation. The performances are compared against a naive baseline without utilizing text information (Methods Sec. 4). **e**, Concordance of MADRIGAL-LLM trained on only training data (same as (c-d)) with a MADRIGAL model trained on all data, as measured by Spearman's rank correlation for unseen safety outcomes across the different text descriptions types. Only those safety outcomes and description types that are significantly correlated ($p\text{-value} < 0.05$) are shown. Data in the methemoglobinemia (first) row are clamped at $x = 0$ for ease of visualization. **f**, Using MADRIGAL-LLM for realistic query of drug pairs and an outcome description related to anemia. The results are summarized in the rightmost panel.

Online Methods

The Methods section discusses (1) Data used in model development and benchmarking, model validation, and case studies; (2) Details about the architecture and optimization of MADRIGAL; and (3) Details about model validation and pharmacological applications.

1 Datasets

Here, we describe the collection and preprocessing of drug combination data, compound modality data, external datasets used for model evaluation, and information on pharmacological applications.

1.1 Drug Combination Safety Dataset

We collect datasets from TWOSIDES (2019-11) [45] and DrugBank (2023-01-04) [46]. TWOSIDES is a database derived from the FDA Adverse Event Reporting System (FAERS). FAERS is a comprehensive repository of adverse event and medication error reports submitted to the FDA. To ensure the reliability and relevance of our data, we adhere to widely accepted criteria in the existing literature on drug safety data mining [127, 128]. These criteria include: (1) a minimum of three reports for the pair of drugs that report the side effect; (2) a proportional reporting ratio of at least 2; (3) a mean reporting frequency of 0.01 or higher; and (4) a chi-square value of 3.841 or higher ($p\text{-value} \leq 0.05$). Applying these criteria and filtering out safety outcomes with less than 100 samples [50], we have compiled a total of 4,656,138 samples, which include 1,457 unique drugs and 795 unique safety outcomes.

In addition, we also collect data from DrugBank (2023-01-04) [46]. Concretely, we extract raw drug interaction statements from the XML dump and extract drugs and the safety outcome from those statements with manually specified regular expression patterns. The extracted safety outcomes are then manually examined, those that differ by rephrasing are grouped, and the directionality between the two drugs in the statement is neutralized. For example, “@Drug1 increase the QTc-prolonging activities of @Drug2” is grouped with “The risk or severity of QTc prolongation can be increased when @Drug1 is combined with @Drug2”. We filter extracted data to (1) only contain small-molecule drugs with valid SMILES and (2) only include safety outcomes that have more than 20 drug pairs annotated. Applying these criteria, we have compiled 1,188,371 samples, covering 3,632 drugs and 158 unique safety outcomes.

Supplementary Fig. S1 shows the number of drugs with different modality availability, the distributions of the number of safety outcomes per unique drug pair, and the distributions of the number of drug pairs per unique safety outcome.

1.2 Drug Data Modalities

We mainly consider four main “views” about a small molecule compound, each offering a unique modality of information:

1. *Structure* (struc.): As we focus on small-molecule compounds, structural information is essential and is universally available, represented by SMILES strings. These strings are converted into unique molecular graphs using the RDKit package [129].
2. *Pathways-based KG* (PKG): We incorporate biomedical knowledge at the pathway level from the drug-centric precision medicine knowledge graph, PrimeKG [90]. This resource provides interaction profiles between approved drugs and diseases or proteins, and higher-order interactions with biological pathways. We exclude all drug-drug interactions and drug-phenotype interactions (individual drug side effects) to avoid information leakage.
3. *Cell viability profile upon drug perturbation* (CV): We utilize cell viability profiles from the PRISM Repurposing 19Q4 dataset [17] available at [DepMap](#). This dataset includes cell-line screens of chemical perturbation viability for 4,518 compounds against 578 cell lines. We use the preprocessing pipeline from [29], resulting in a 559-dimensional characteristic vector for each compound, with each entry corresponding to the change in viability of a cell line.
4. *Transcriptomics profile upon drug perturbation* (trans.): We gather transcriptomics profiles from the Extended CMap 2020 dataset available at [Connectivity Map](#) [16]. We apply a quality control pipeline adapted from [130]. We select profiles from representative cell lines from each cell lineage and primary disease (among cell lines where more than 500 compounds are screened after filtering) and treat each cell line as a separate modality. In total, 16 cell lines are selected (as specified below). For each compound, within each cell line and treatment time, following recommendations in [131], we select the profiles from the maximal dosage applied. We adapt the pipeline in [132], where molecules are selected if they have more than five replications (irrespective of the cell line, treatment time, dose, and plate). Repetitions and plates are averaged. We concatenate profiles for each compound at two treatment times, namely 24h and 6h. The resulting input from each modality is a $(2 \times 978 =)$ 1956-dimensional feature vector, with two entries corresponding to the expression change of a landmark gene at two-time stamps.

We match data from these modalities based on the RDKit-transformed canonical SMILES, each uniquely identifying a compound. Drug interaction data are mapped to compounds via DrugBank ID. Fig. 1c and Supplementary Fig. S1 provides an overview of the availability of drug data across these modalities.

1.3 Drug-Induced Liver Injury (DILI) Datasets

Using names and SMILES, we match drugs in the DILI dataset curated by [54] to DrugBank identifiers in our data. This yields 262, 234, 217, and 159 drugs with minor, no, ambiguous, and most severe DILI concerns, respectively.

1.4 Drug-Induced Cardiotoxicity (DICT) Dataset

Using names and SMILES, we match drugs in the DICT dataset curated by [55] to DrugBank identifiers in our data. This yields 301, 236, 68, and 206 drugs with minor, no, ambiguous, and most severe DICT concerns, respectively.

1.5 Drug-Induced QTc Prolongation (DIQTA) Dataset

Using names and SMILES, we match drugs in the DIQTA dataset curated by [56] to DrugBank identifiers in our data. This yields 55, 241, 100, and 109 drugs with moderate, no, ambiguous, and most severe DIQTA concerns, respectively.

1.6 Type II Diabetes Comorbidity Drugs

We have also curated an extensive dataset of disease comorbidities used in our case studies, where we examine specific diseases, such as Type II Diabetes (T2D). The main comorbidities dataset is created by combining pre-existing datasets from FAERs [133] and Type I and Type II Diabetes datasets [134]. The FAERs dataset consists of common disease comorbidities extracted from FDA's Adverse Event Reporting System using Association Rule Mining (2014 - 2017), with 25215 disease pairs, which includes 20159 unique diseases. Type I and Type II diabetes comorbidities were extracted from Austria patients from 2006 - 2007; comorbidities were calculated through risk ratios (RR), and disease pairs with an RR of at least 2.0 were considered comorbid. With that comorbidity calculation metric, there were 391 T1D comorbidity pairs, which included 829 unique diseases, and 265 T2D comorbidity pairs, which included 937 unique diseases. However, when examining specific diseases (MASH, heart failure, and kidney diseases), we note that they appear in our curated comorbidity dataset but are not included in PrimeKG [90] due to compatible identification mapping. Thus, not all diseases in a specific class are examined, even though they might appear in the comorbidities dataset; only

diseases in our comorbidity dataset and PrimeKG are used in the following analyses.

T2D medications are sourced from DrugCentral through PrimeKG [90], the FDA Orange Book, and supplemented with mechanism of action data from UCSF [91], Mayo Clinic [92], and Cleveland Clinic [93]. We ensure that all medications, if not approved in the US, are marketed in Europe or Japan. Although we focus primarily on small-molecule drugs and exclude insulin and its analogs, we include GLP-1 receptor agonists such as semaglutide, cotadutide, and lixisenatide, with available SMILES data. The complete list of drugs is shown in Supplementary Table S3. Similarly, HF medications are sourced from the American Heart Association and the Orange FDA book. The complete list of drugs is shown in Supplementary Table S4.

1.7 MASH Combination Therapies

We obtain the MASH clinical candidates and approved drugs, including monotherapies [88, 103] and combination therapies [84, 85, 108]. The MOAs and clinical phases are manually annotated by extracting information from the references above. Only small-molecule drugs with valid SMILES are considered. The specific candidates included and their MoAs are shown in Supplementary Table S5, and also in Fig. 5h and Supplementary Fig. S6d.

1.8 Cancer Drugs and PARPi Combination Therapies Dataset

We collect PARPi's that are FDA-approved or currently under advanced stages of clinical trials that are sufficiently represented (with at least five different other drugs) for at least two outcomes in our dataset. Three PARPi's are collected of this kind, namely olaparib, talazoparib, and rucaparib, which are associated with 11, 6, and 9 outcomes, respectively.

We then filter curated approved or clinically investigated PARPi combinations in [64, 73, 78] so that both drugs in each combination are present in our data. This filters out non-small-molecule drugs, leaving us with nine combinations for olaparib, 1 combination for talazoparib, and 1 combination for rucaparib.

To curate a list of drugs indicated for cancer, we consider cancer drugs collected by [135] (version 07/02/2024), whose source data comes from the NCI, FDA, EMA, and others. According to the authors, “The intention is to provide researchers, clinicians, and regulators with an easily filtered database of licensed drugs used to treat cancer. Drugs used in cancer treatments to alleviate symptoms or other supportive care uses or used for diagnostic purposes are not included. Investigational agents and experimental treatments used in clinical trials are also not included.” This list is supplemented by two other sources (excluding PARPi's):

- Drugs whose ATC codes start with L. As drugs falling under the L02, L03, and L04

classification might have non-cancer indications, we further ensure that these L02, L03, or L04 drugs have cancer-related descriptions in their description, mechanism of action, or indication in DrugBank [46] or DepMap [17].

- Drugs indicated for cancer as curated in DrugCentral [89], obtained through PrimeKG [90].

We manually examined all drugs that are not approved in the US. We ensured that they are currently approved in Europe, Japan, South Korea, China, Australia, or Germany or are in an advanced stage of clinical trials (at least phase 3) and not discontinued due to safety or efficacy and not with a withdrawal history, using DrugBank and Synapse [136]. In total, we collect 288 cancer drugs of interest. For all drugs, the categorical mechanism of action annotations are extracted from DepMap [17] and CMap [16], and the target annotations are extracted from DrugBank. The specific drug names and their DrugBank IDs are provided in Supplementary Table S2.

The clinically-investigated PARPi combinations are curated from [78].

1.9 BeatAML Ex Vivo Drug Synergy Dataset

We obtain the latest BeatAML ex vivo drug synergy dataset courtesy of Dr. Jeffrey Tyner, which is an updated dataset of similar outcome measurement as in [39, 40], comprising more patients and drug combinations tested. The data preprocessing was done in the same approach as in [39], courtesy of Dr. Christopher Eide. We further filter the data so that only patients with RNA-seq profiles and small-molecule drug information are included. This gives us 336 patient samples, 135 drug combinations, and 12,161 (patient sample, drug combination) pairs.

Following the original BeatAML paper [40], the synergy measure we use is combination ratio (CR), defined as the AUC (percentage of max) of the drug combination divided by the minimum AUC of each drug in the combination. A CR lower than 1 represents synergy pairs, and vice versa. The drugs in the dataset are matched with DrugBank ID based on their names.

1.10 Patient-derived Xenograft Drug Combination Dataset

We obtain the patient-derived xenograft encyclopedia (PDXE) dataset from [41]. We further filter the data so that only patients with RNA-seq profiles and small molecule drugs with structural information available are included. This gives us 171 models, 11 drug combinations, and 366 (model, drug combination) pairs. An overview of the data is presented in Supplementary Fig. S7.

The efficacy measures we use are TimeToDouble, which corresponds to progression-free survival (time until tumor volume reaches 200% of baseline), and BestAvgResponse, which

corresponds to response (minimum value of the average of ΔVol_t from $t = 0$ to T , for $T \geq 10$ d). The drugs in the dataset are mapped to DrugBank ID by name and through manual confirmation with literature.

2 MADRIGAL Model

We aim to utilize compounds with incomplete information or without combination safety information to inform the understanding of drugs that lack specific modalities. To achieve this, we focus on pretraining the model so that the modality-specific representations of drugs, encoded by various encoders, are aligned. Intuitively, once we have well-aligned representations from different modalities, the representations derived from a subset of available modalities of a compound should retain shared information from the missing modality. By ensuring an aligned initialization of encoders, we circumvent the pitfalls of random model initialization, which has been shown to lead to the undesirable phenomenon of modality competition [35].

2.1 Problem Setup and Notation

Let $\mathcal{D} = \{d_i\}_{i=1}^{n_D}$ denote the set of compounds available to us with either multiple modalities of information or a combination of safety information available. For the subset of drugs in \mathcal{D} that have combination safety information available, a sample is defined by (d_1, d_2, r) where $d_1, d_2 \in \mathcal{D}$ are two compounds and $r \in \mathcal{R}$ is a type of combination outcome. Each compound $d_i \in \mathcal{D}$ is uniquely identified by a SMILES string x_i^{smiles} and characterized by at most $n_M = 19$ modalities, namely:

- struc.: represented by a molecular graph, $x_i^{\text{struc}} = (\mathcal{V}_{x_i}, \mathcal{E}_{x_i}, \mathbf{X}_{x_i}, \mathbf{E}_{x_i})$ (generated from x_i^{smiles})
- PKG: represented by a drug node and its neighborhood or computation tree on a drug-centered knowledge graph G , $x_i^{\text{PKG}} = (d_i, G)$
- CV: represented by a perturbation profile, $x_i^{\text{CV}} \in \mathbb{R}^{559}$
- trans.-{cell line} ($\{\text{cell line}\}$ denotes one of the 16 cell lines we collected, for example, MCF7): represented by a perturbation profile, $x_i^{\text{trans.-}\{\text{cell line}\}} \in \mathbb{R}^{1956}$

Denote the full set of modalities as $\mathcal{M} = \{\text{struc., PKG, CV, trans.-MCF7, trans.-VCAP, trans.-PC3, trans.-A549, trans.-A375, trans.-HA1E, trans.-HT29, trans.-HCC515, trans.-NPC, trans.-HELA, trans.-HEC108, trans.-THP1, trans.-HEPG2, trans.-YAPC, trans.-ASC, trans.-HUVEC}\}$. Also, denote the set of modalities available to a compound d as $\mathcal{M}_d \subseteq \mathcal{M}$. For each modality

$m \in \mathcal{M}$, a modality-specific encoder $f^m : \mathcal{X}^m \rightarrow \mathbb{R}^{\text{shared}}$ maps the modality-specific data to representations in a shared latent space. Note, for simplicity, through the following development, we denote transcriptomics as one modality (trans.), while it is treated as 16 modalities (each cell line as one) in the model.

2.2 Three-stage optimization

Our model architecture, designed to handle any composition of compound modalities as input and predict safety profiles for drug combinations, is depicted in Fig. 1. The model’s encoder components are first initialized and adapted with encoder-specific pretext tasks. They are then pretrained with a contrastive objective and transferred to the downstream finetuning for combination safety prediction. The model architecture and learning objectives are formally defined in the following subsections and optimized sequentially in three stages.

2.2.1 Initializing and adapting individual modality-specific encoders

For each modality, we employ modality-specific state-of-the-art encoders. Specifically, we utilize a Heterogeneous Graph Transformer [137] encoder for the pathways-based KG modality, a Graph Isomorphism Network [138] backbone encoder for the molecular structure modality, a multilayer perceptron for the cell viability upon perturbation modality (only using the encoder part when encoding), and one chemCPA [139] encoder (with RDKit descriptor and no dosage) for all transcriptomics perturbation modalities. To allow encoders to produce meaningful representations before alignment, we initialize encoder f^m for each modality $m \in \mathcal{M}$ from scratch and adapt them with individual modality-specific pretext tasks.

- struc.: A supervised property prediction task is used to train the structure encoder. Let $y^{\text{struc.}}$ denote the measurement of some property of interest for compound d . We apply a linear head $h^{\text{struc.}}$ above the structural encodings to predict 17 properties for about 90k molecules from PubChem BioAssay [140] compiled by the MoleculeNet benchmark as the Maximum Unbiased Validation (MUV) dataset [141]. We then optimize f^{str} by minimizing a mean square error loss, i.e.

$$L_{\text{MSE}}^{\text{struc.}} = \frac{1}{n_{\text{struc.}}} \sum_{i=1}^{n_{\text{struc.}}} (h^{\text{struc.}}(f^{\text{struc.}}(x_i^{\text{struc.}})) - y^{\text{struc.}})^2$$

- PKG: A self-supervised knowledge graph link prediction task is used to train the pathways encoder. In this task, we predict the existence of edges between two nodes in the knowledge graph G (removing all drug-drug and drug-phenotype edges). Let E denote all such edges, N denote negative samples and h^{PKG} denote the scoring function for link

prediction from a triplet of $(f^{\text{PKG}}(s, G), f^{\text{PKG}}(t, G), r)$, where s is the source node, t is the target node and r is the edge type. We optimize f^{PKG} for minimizing a binary cross-entropy loss, i.e.

$$L_{\text{BCE}}^{\text{PKG}} = \frac{1}{n_{\text{PKG}}} \left(- \sum_{(s,t,r) \in E} \log h^{\text{PKG}}(f^{\text{PKG}}(s, G), f^{\text{PKG}}(t, G), r) \right. \\ \left. - \sum_{(s,t,r) \in N} (1 - \log h^{\text{PKG}}(f^{\text{PKG}}(s, G), f^{\text{PKG}}(t, G), r)) \right)$$

- CV: A reconstruction [142] objective is used to train the CV encoder. The encoder compresses the input information into a latent representation from which the decoder reconstructs the input. Specifically, f^{CV} encodes x^{CV} as latent vector z^{CV} , while h^{CV} decodes z^{CV} to reconstruct x^{CV} . In practice, we train the model to minimize the mean square error loss:

$$L_{\text{MSE}}^{\text{CV}} = \frac{1}{n_{\text{CV}}} \sum_{i=1}^{n_{\text{CV}}} (h^{\text{CV}}(f^{\text{CV}}(x_i^{\text{CV}})) - x_i^{\text{CV}})^2$$

- trans. (trans.-{cell lines}): We pretrain the encoder with a strategy similar to chemCPA despite removing the drug adversarial loss on our dataset as we intend to learn drug representations instead of making counterfactual predictions. We refer interested authors to [139] for details about their training objective.

2.2.2 Modality alignment with multimodal contrastive learning

In this stage, our objective is to align the representations generated for the same drug from different modalities with the structure modality with a multimodal contrastive representation learning objective. We adopted the InfoNCE objective [143] with minor modifications similar as in [144], and jointly learn all encoders $f^m, m \in \mathcal{M}$, initialized from stage 1, s.t. the loss

$$L_{\text{cont}} = \sum_{m \neq \text{struc.}} L(m, \text{struc.}) = \sum_{m \neq \text{struc.}} (\ell(m, \text{struc.}) + \ell(\text{struc.}, m)),$$

where

$$\ell(m_u, m_v) = - \sum_{i=1}^B \log \frac{\text{sim}_{(m_u, m_v)}(d_i, d_i)}{\sum_{j=1}^B (\text{sim}_{(m_u, m_v)}(d_i, d_j) + \mathbf{1}_{j \neq i} \cdot \text{sim}_{(m_u, m_u)}(d_i, d_j))},$$

and

$$\text{sim}_{(m_u, m_v)}(d_i, d_j) = \exp(f^{m_u}(d_i) \cdot f^{m_v}(d_j)/\tau),$$

is minimized.

In implementation, we randomly sample the other modality (other than structure) for each compound, with the probability inversely proportional to the modality’s availability, measured by its prevalence in the pre-training set of compounds.

2.2.3 Additional note on modality alignment

Concretely, let $z_{\text{struc.}}, z_{\text{PKG}}, z_{\text{CV}}, z_{\text{trans.}}$ be modality-specific representations encoded by respective encoders f^m , where $m = \text{struc.}, \text{PKG}, \text{CV}, \text{trans.}$, as defined before. A careful reader might note that the structure modality is anchor-like in the contrastive objective above. Minimizing the sum of InfoNCE objectives between the structure modality and other modalities, respectively, can be viewed as maximizing a lower bound estimate of the sum of mutual information shared between representations of the structure modality and other modalities, respectively [145], i.e.,

$$\max_{\{f^m\}_{m \in \mathcal{M}}} \sum_{m \neq \text{struc.}} I(z_{\text{struc.}}; z_m),$$

where I denotes mutual information, which directly aims to align the structure modality with all other modalities. Under the assumption of conditional independence structure between other modalities given the structure modality, i.e. $z_{\text{CV}} \perp z_{\text{PKG}} \mid z_{\text{struc.}}, z_{\text{trans.}} \perp z_{\text{PKG}} \mid z_{\text{struc.}}, z_{\text{trans.}} \perp z_{\text{CV}} \mid z_{\text{struc.}}$, the pairwise mutual information objective is equivalent to:

$$\max_{\{f^m\}_{m \in \mathcal{M}}} \sum_m H(z_m) - H(z_{\text{struc.}}, z_{\text{PKG}}, z_{\text{CV}}, z_{\text{trans.}}),$$

where H denotes entropy, it can thus be interpreted that the maximization of $\sum_m H(z_m)$ ensures that each modality retains its inherent variability and richness, and the minimization of $H(z_{\text{struc.}}, z_{\text{PKG}}, z_{\text{CV}}, z_{\text{trans.}})$ as ensuring that the joint representation is compact and has lower redundancy.

2.2.4 Model finetuning

Given the impressive performance of attention-based fusion in other multimodal learning contexts, particularly in vision-language models [44, 146, 147], and their flexibility of inputs, we adopt a Transformer encoder architecture for modality fusion to model the joint representations across modalities. We apply self-attention without incorporating cross-modal attention in individual encodings, which reduces computational overhead, fits into our relatively small sample size, and enables a flexible composition of modality inputs. To address the high number of modalities that fall under the transcriptomics upon perturbation category, we insert bottleneck tokens and restrict attention thereafter (Supplementary Fig. S1b). The output bottleneck token embeddings are max-pooled to generate a multimodal drug embedding. Unless explic-

itly mentioned (as in the case of MADRIGAL-LLM), a bilinear decoder is used for scoring the probabilities of a pair of compounds having any safety outcomes for computational efficiency.

Denote a flexible fusion module as g^{fusion} , which maps any one or combination of modality-specific encodings for compound d : $\{f^m(x^m)\}_{m \in \mathcal{M}_d}$ to a single compound encoding $\mathbf{z}^{\mathcal{M}_d} \in \mathbb{R}^{\text{joint}}$. Denote as $h^{\text{dec}} : \mathbb{R}^{\text{joint}} \times \mathbb{R}^{\text{joint}} \times \mathcal{R} \rightarrow [0, 1]$ the decoder for the prediction of safety outcomes from the multimodal encodings of drugs. Let S denote all samples, and S_{neg} denote all negative samples. We then jointly optimize all encoders f^m (initialized from stage 2) and $g^{\text{fusion}}, h^{\text{dec}}$ (both randomly initialized), s.t. the loss

$$L_{\text{BCE}}^{\text{ft}} = \frac{1}{|S|} \left(- \sum_{(d_1, d_2, r) \in S} \log h^{\text{dec}}(g^{\text{fusion}}(\{f^m(d_1^m)\}_{m \in \mathcal{M}_{d_1}}), g^{\text{fusion}}(\{f^m(d_2^m)\}_{m \in \mathcal{M}_{d_2}}), r) \right. \\ \left. - \sum_{(d_1, d_2, r) \in S_{\text{neg}}} \left(1 - \log h^{\text{dec}}(g^{\text{fusion}}(\{f^m(d_1^m)\}_{m \in \mathcal{M}_{d_1}}), g^{\text{fusion}}(\{f^m(d_2^m)\}_{m \in \mathcal{M}_{d_2}}), r) \right) \right)$$

is minimized.

2.2.5 Implementation details

At the third stage of model training, we finetuned the encoders, fusion module, and decoder on the combination safety prediction task, with encoders initialized from a pretrained model checkpoint. We used the AdamW optimizer for all three stages and followed a linear warm-up with a cosine annealing schedule, a common practice in training multimodal models.

Hyperparameter tuning. We leverage Weights and Biases [148] to select optimal hyperparameters via a random search over the hyperparameter space. The best-performing hyperparameters are selected by optimizing the AUPRC on the validation set. The hyperparameter space on which we perform a random search to choose the optimal set of hyperparameters is: position embedding \in [learnable, sinusoidal], position embedding dropout $\in [0.1, 0.2, 0.4]$, number of heads in transformer encoder $\in [2, 4, 8]$, dimension of heads in transformer encoder $\in [64, 128, 256]$, number of layers in transformer encoder $\in [2, 3, 4, 6]$, dimension of feed forward layer in transformer encoder $\in [256, 512, 1024]$, dropout in transformer encoder $\in [0.2, 0.3, 0.4]$, number of attention bottlenecks $\in [2, 4]$, dropout in projector $\in [0.1, 0.2, 0.4]$, warmup epochs $\in [10, 20, 50, 100]$, learning rate (for each of structure encoder, pathways encoder, cell viability and transcriptomics encoder, fusion module, decoder) $\in [1e-4, 5e-4, 1e-3, 5e-3]$, weight decay $\in [0.001, 0.01, 0.1]$, epsilon $\in [1e-8, 1e-7, 1e-6]$, whether or not having a separate adaptor when the drug only has one (structure) modality available, and the ordering of dropout and normalization layer (i.e., normalization before dropout, or vice versa).

To reduce cost, we only tune hyperparameters for each dataset using one splitting strategy (split-by-drugs (random)). The optimal sets of hyperparameters selected are:

- DrugBank dataset: position embedding = `sinusoidal`, position embedding dropout = 0.2, number of heads in transformer encoder = 8, dimension of heads in transformer encoder = 64, number of layers in transformer encoder = 2, dimension of feed-forward layer in transformer encoder = 256, dropout in transformer encoder = 0.3, number of attention bottlenecks = 4, dropout in projector = 0.1, warmup epochs = 100, learning rate (for each of structure encoder, pathways encoder, cell viability and transcriptomics encoder, fusion module, decoder) = $1e-4, 1e-3, 1e-4, 1e-3, 1e-3$, weight decay = 0.001, epsilon = $1e-6$, no separate projector for when the drug has only one (structure) modality available, and normalization layer first.
- TWOSIDES dataset: position embedding = `sinusoidal`, position embedding dropout = 0.2, number of heads in transformer encoder = 8, dimension of heads in transformer encoder = 256, number of layers in transformer encoder = 2, dimension of feed-forward layer in transformer encoder = 1024, dropout in transformer encoder = 0.2, number of attention bottlenecks = 2, dropout in projector = 0.2, warmup epochs = 100, learning rate (for each of structure encoder, pathways encoder, cell viability and transcriptomics encoder, fusion module, decoder) = $5e-3, 5e-3, 1e-4, 1e-4, 1e-4$, weight decay = 0.1, epsilon = $1e-7$, separate projector for when the drug has only one (structure) modality available, and normalization layer first.

Implementation. We implement all MADRIGAL models using Pytorch (Version 1.12.1) [149]. We used Weights and Biases [148] for hyperparameter tuning and visualization of model training. MADRIGAL models are trained on a single NVIDIA A100 GPU. When predicting drug combination synergy in the BeatAML dataset, gradient boosting classifiers are implemented using scikit-learn [150] and trained on the CPU.

MADRIGAL is computationally efficient due to the relatively small computation overhead and the feasibility of fitting the entire dataset to a single GPU with efficient operations, taking only a few hours to fine-tune the DrugBank data set on an A100 GPU, compared to the days required by many strong baselines (Supplementary Fig. S2).

3 Benchmarking MADRIGAL Model

3.1 Dataset Splits

As novel compounds typically lack combination safety information, we held out (about) 20% approved drugs in each dataset, along with their associated combinations, to rigorously evaluate model performance under realistic conditions. To achieve this, we designed three distinct testing scenarios using different data splitting strategies: based on drug ATC codes (“split-by-drugs (atc)”), drug targets (“split-by-drugs (target)”), random splits by drugs (“split-by-drugs (random)”). In each splitting setting, we also additionally split (about) 10% drugs into a validation set to prevent model overfitting and for hyperparameter tuning. In addition, to evaluate the model also in a more traditional setting, in the fourth strategy, we randomly split 20% drug pairs and all associated combinations into a test set (“split-by-drug pairs”), 10% drug pairs and all associated combinations into validations set, and rest in the training set.

In the three split-by-drugs settings, training samples are formed by selecting those samples where both drugs are in the train set. However, there is a unique aspect for validation or test samples in these settings: for each validation or test drug, the other drugs it interacts with could either be in the validation or test or included in the train set. These two types of samples have different implications: one scenario mimics the case where both drugs are novel compounds, while the other can be viewed as the scenario where one drug is a novel compound and the other is an approved drug. In practice, it is more valuable to understand the interaction profiles of a novel compound with approved drugs in related therapeutic areas (such as comorbidities). Therefore, we focus on the latter group of samples when evaluating the model. Specifically, validation samples are formed by selecting those samples where one drug is in the validation set while the other is in the train set; test samples are formed by selecting those samples where one drug is in the test set while the other is in the train or validation set.

In the split-by-drugs (ATC) setting, drugs in each dataset are grouped according to the initial letter of their ATC codes (anatomical or pharmacological groups). ATC codes are randomly split into train, validation, and test sets. For the DrugBank dataset, drugs whose ATC codes start with “N”, “V”, “J”, “B”, “C”, “A” are split into train set, containing a total of 2589 drugs and 584,891 samples, drugs whose ATC codes start with “D”, “L” are split into validation set, containing a total of 433 drugs and 162,608 samples, drugs whose ATC codes start with “G”, “H”, “M,” “R”, “P”, “S” are split into test set, containing a total of 670 drugs and 368,646 samples. For the TWOSIDES dataset, drugs whose ATC codes start with “H”, “L”, “G”, “S”, “D”, “A”, “N”, “J”, “M”, are split into train sets containing a total of 1043 drugs and 2,084,566 samples, drugs whose ATC codes start with “R”, “P” are split into validation set, containing a

total of 149 drugs and 747,959 samples, and drugs whose ATC codes start with “B”, “V”, “C” are split into test set, containing a total of 276 drugs and 1,478,489 samples.

In the split-by-drugs (target) setting, because each drug can have multiple targets, which makes naively splitting targets infeasible, we construct a drug network where two drugs are connected if they share any target. The largest connected component (LCC) contains more than half (DrugBank dataset: 52%; TWOSIDES dataset: 66%) of drugs with target profiles, which we then detect communities (DrugBank dataset: 14; TWOSIDES dataset: 9) via the Louvain algorithm. The communities from LCC, along with other components in the network, are randomly split such that 20% of drugs are in the test set, 10% of drugs are in the validation set, and others are in the train set. All drugs without target information in DrugBank are split into train sets. Specifically, for the DrugBank dataset, 2482, 423, 727 drugs are split into train, validation, and test sets, containing a total of 426,890, 264,272, 381,841 samples, respectively; for the TWOSIDES dataset, 987, 156, 314 drugs are split into train, validation, and test sets, containing a total of 1,923,741, 669,568, 1,706,453 samples, respectively.

In the split-by-drugs (random) setting, we randomly divided the drugs in each dataset into train, validation, and test sets with the ratios above. For the DrugBank dataset, the train, validation, and test sets contain 565,166, 170,888, and 388,492 samples, respectively; for the TWO-SIDES dataset, the train, validation, and test sets contain 2,345,947, 664,265, and 1,432,496 samples, respectively.

In the drug pair splits, we randomly divided drug pairs in each dataset into train, validation, and test sets with the ratios above. For the DrugBank dataset, the train, validation, and test sets contain 831,859, 118,837, and 237,675 samples, respectively; for the TWOSIDES dataset, the train, validation, and test sets contain 3,254,433, 466,311, and 935,394 samples, respectively.

3.2 Experimental Setup

For MADRIGAL only, we also artificially removed the knowledge graph modalities for test drugs, allowing us to simulate the realistic scenario where much of the clinical and postmarketing information about novel compounds is not available. MADRIGAL is trained with five different seeds (0, 1, 2, 42, 99) for each splitting strategy, and average performances with standard deviations are presented in all benchmarking tables.

We also ablate MADRIGAL in three ways:

1. w/o CL: Training the model directly on the combination safety dataset without modality alignment.

2. struc. only: Only using structure modality during model finetuning (but with all modalities during modality alignment).
3. struc. only w/o CL: Training the model directly on the combination safety dataset using only structure modality, without modality alignment.

3.3 Evaluation Metrics

We evaluate model performance with standard classification metrics, including the area under receiver-operating curve (AUROC), the area under the precision-recall curve (AUPRC), and maximum F-measure (Fmax), calculated in a “macro” manner, i.e., within each label (safety outcome) then averaged. Such averaging approach is in practice more useful than “micro” (i.e. flattening predictions across all labels and calculate metric over all predictions), which compares predictions across labels and might not be meaningful without appropriately encoding information about safety outcomes (for example, with a language model).

Specifically, for each outcome, given predicted scores $\mathbf{s} = (s_1, s_2, \dots, s_N)$ and corresponding binary labels $\mathbf{y} = (y_1, y_2, \dots, y_N)$, Fmax is calculated as:

$$F_{\max} = \max_{\tau} F(\tau),$$

where the F1 score at threshold τ is defined as

$$F(\tau) = \frac{2 \operatorname{Prec}(\tau) \operatorname{Rec}(\tau)}{\operatorname{Prec}(\tau) + \operatorname{Rec}(\tau)},$$

with the precision and recall at threshold τ being

$$\operatorname{Prec}(\tau) = \frac{\sum_{i=1}^N y_i \mathbb{I}(s_i \geq \tau)}{\sum_{i=1}^N \mathbb{I}(s_i \geq \tau)}, \quad \operatorname{Rec}(\tau) = \frac{\sum_{i=1}^N y_i \mathbb{I}(s_i \geq \tau)}{\sum_{i=1}^N y_i},$$

where $\mathbb{I}(\cdot)$ is the indicator function.

Following benchmarking setups in previous literature [50, 51, 53], for each (drug 1, drug 2, outcome) sample, we obtain negative samples by randomly sampling a drug (drug 2') to replace drug 2 and a drug (drug 1') to replace drug 1, forming two negative samples (drug 1, drug 2', outcome) and (drug 1', drug 2, outcome). We also ensure the negative samples do not exist in the dataset.

In certain analyses, we also calculate metrics for each test drug. This is done by calculating metrics within all test samples containing the test drug and all corresponding negative samples.

3.4 Baselines

To test the performance of our proposed MADRIGAL, we compare MADRIGAL with six baselines across four modalities on two datasets.

DeepDDI [151] is a structure-based DDI prediction model. It uses a deep neural network to predict drug combinations from drug structural information. It has been shown to predict adverse drug interactions involving SARS-COV-2 therapies [48].

CASTER [49] is inspired by drug chemical substructures. It first extracts frequent substructures from a molecular database. Then, it designs a latent feature embedding module to represent drugs in terms of the extracted frequent substructures and predict drug combinations.

GMPNN-CS [50] predicts drug combinations by learning chemical substructures with different sizes and shapes from the molecular graph representations of drugs. It considers the edge between atoms as gates that control the flow of message passing and, therefore, delimit the substructures in a learnable way.

DDKG [51] predicts potential drug combinations based on drug representations learned from KG by GCN. Besides that, DDKG also integrates drug SMILES into DDI predictions by initializing drug embeddings with SMILES.

MUFFIN [52] explores the joint effect of drug molecular structures and semantic information of drugs in KG for DDI prediction. It predicts drug combinations by jointly learning the drug representation based on the drug-self structure information and the KG with rich biomedical information.

TIGER [53] is a transformer-based DDI prediction model. It predicts potential drug combinations based on drug molecular graphs and KGs. TIGER extends the transformer to graph-level and node-level representation learning, thus finishing drug combination predictions.

3.5 Modality Ablation Tests

In this study, we utilize various modalities—such as drug structures, pathways, cell viability profiles following drug perturbations, and transcriptomics profiles after drug perturbations—to predict drug combinations. To assess the effectiveness of these modalities, we conduct an ablation study by removing each modality one at a time and testing the model’s model’s performance with the remaining modalities. By comparing the performances with and without specific modalities, we can identify which ones are most critical for model performance.

4 MADRIGAL-LLM Extension

4.1 Augmenting descriptions of drug combination outcomes

We use GPT-4 to get augmented and diverse safety outcome descriptions [152]. The original descriptions from DrugBank are short and formulaic, which makes the model unable to learn more flexible representations of safety outcome descriptions. We design a prompt that engages GPT-4 using the gpt-4-0125-preview API version with a knowledge cutoff of December 2023 to return the augmented version of each safety outcome description as a medical doctor, pharmacologist, and toxicologist. In the prompt, we ask it not to hypothesize anything about the drug types or methods of action and to restrict it to augmenting just the safety outcome description. There are 269 unique descriptions from DrugBank for the 158 outcomes in the DrugBank dataset, as some classes can have more than one description. We generate three different augmentations for each expert for each class, totaling nine augmented descriptions per class.

We use the following prompt for augmenting descriptions:

Your task is to take original descriptions of drug-drug interactions and augment them. Make sure the information you provide is correct and valid, and the extended text is two sentences long. To ensure diversity in these descriptions, respond as each of the following: medical doctors (physician), pharmacologist and toxicologist. Medical doctors: Especially those specializing in fields such as pharmacology, internal medicine, and clinical pharmacology. Hence, they understand the symptoms and organ systems affected due to the drug-drug interaction. Pharmacologists: Scientists who study the effects of drugs on biological systems. They understand the genetic and molecular mechanism behind these interactions. Toxicologists: Scientists typically work with chemicals and other substances to determine if they are toxic or harmful to humans, other living organisms, or the environment. Your job is to generate nine versions of the original description (given below after ‘Original description’) - three for each profession and at the correct level of understanding and expertise. Your responses for the scientists should be diverse in terms of style, length, and language used. Each of the scientist’s responses must be different in terms of the level of vocabulary used, sentence structure, and word choice. None of the nine responses can be the same or have any repeating sentences. Please also make sure you do not make any assumptions about @Drug1 and @Drug2. An example output is given for you after ‘Example’. The description to augment is given after ‘Task’. Example: Description: The risk or severity of bleeding and bruising can be increased when @Drug1 is combined with @Drug2. Output: {"medical_doctor_1": "When @Drug1 is combined with @Drug2, there is an elevated risk of experiencing increased bleeding and bruising, a concern particularly for

patients with pre-existing bleeding disorders or those on anticoagulant therapy. These patients should be closely monitored for any signs of abnormal bleeding and adjustments to therapy may be necessary.”, “medical_doctor_2”: “The concurrent use of @Drug1 with @Drug2 can lead to a heightened risk or severity of bleeding and bruising, necessitating careful consideration in patients undergoing surgical procedures or those with a history of bleeding problems. Its vital to evaluate the benefits and risks of continuing this drug combination in such contexts.”, “medical_doctor_3”: “Combining @Drug1 with @Drug2 can significantly increase the likelihood of bleeding and bruising, an issue of particular concern for individuals with liver impairment or those consuming alcohol regularly. These patients may require dose adjustments or more frequent monitoring to mitigate the risks.”, “pharmacologist_1”: “The interaction between @Drug1 and @Drug2 can escalate the risk of bleeding and bruising due to their synergistic effects on inhibiting platelet aggregation or affecting coagulation pathways. Understanding the molecular basis of this interaction is crucial for predicting patient responses and managing therapy effectively.”, “pharmacologist_2”: “When @Drug1 and @Drug2 are co-administered, they may interfere with each others pharmacokinetic or pharmacodynamic profiles, leading to an increased risk or severity of bleeding and bruising. This interaction suggests a complex interplay at the cellular level, possibly involving the modulation of enzymes or receptors associated with hemostasis.”, “pharmacologist_3”: “The combination of @Drug1 and @Drug2 can intensify bleeding and bruising risks, likely through a mechanism involving the alteration of drug metabolism or the exacerbation of anticoagulant effects. Pharmacologists should explore the specific pathways affected to tailor safer therapeutic strategies.”, “toxicologist_1”: “The interaction between @Drug1 and @Drug2 may elevate the risk of bleeding and bruising by enhancing the toxic effects on the bodys hemostatic system, potentially leading to hazardous conditions such as uncontrolled bleeding. Toxicologists should assess the cumulative impact of these drugs to ensure patient safety.”, “toxicologist_2”: “Co-administration of @Drug1 with @Drug2 can lead to increased toxicity, manifesting as heightened bleeding and bruising, by overburdening the bodys natural mechanisms for blood clotting. This interaction underscores the importance of toxicological evaluation for identifying potential adverse effects on the hemostatic process.”, “toxicologist_3”: “When @Drug1 and @Drug2 are used together, their combined toxic effects can compromise the integrity of the vascular and coagulation systems, increasing the risk of bleeding and bruising. This interaction highlights the need for ongoing monitoring and possibly adjusting dosages to mitigate the toxicological risks involved.”} Task:

Description: {DESC} Output:

4.2 Large language model with MADRIGAL

We start with the aligned modality-specific encoders (after first and second-stage optimization) of MADRIGAL. We use the Mistral 7B [126] model to encode text descriptions of drug-drug interactions. Then, a self-attention layer is applied to the two drug-modality-fused encodings and the text encoding, with an MLP decoder to predict the described safety outcome from the concatenation of self-attention outputs. More specifically,

$$\begin{aligned} z_{d_1} &= \text{MADRIGAL}(x_{d_1}), \\ z_{d_2} &= \text{MISTRAL}(x_{d_2}), \\ z_{\text{text}} &= \text{MISTRAL}(x_{\text{text}}). \end{aligned}$$

Then,

$$\begin{aligned} z &= [z_{d_1}, z_{d_2}, z_{\text{text}}], \\ z_{\text{attn}} &= \text{Self-Attention}(z), \\ y &= \text{MLP}(z_{\text{attn}}). \end{aligned}$$

We keep the LLM parameters frozen during training while the weights of the modality-specific encoders, the modality fusion module, the self-attention layer, and the MLP decoder are updated. A binary cross entropy loss with a positive weight w_p is used to train the model.

$$\mathcal{L} = -\frac{1}{N} \sum_{i=1}^N [w_p y_i \log(\hat{y}_i) + (1 - y_i) \log(1 - \hat{y}_i)] \quad (1)$$

Implementation details.

We trained MADRIGAL-LLM for 20 epochs using an Adam optimizer with a learning rate 2e-5 and a weight decay of 1e-2. We used a training batch size of 3000 and an evaluation batch of 4000. The weight parameter of the Binary Cross Entropy loss was set to 2.4, where the loss from each positive label is weighted 2.4 times more than each negative label.

4.3 Evaluation of MADRIGAL-LLM

We designed a baseline that consider semantic similarity to benchmark the performance of MADRIGAL-LLM, since no other baselines exist in this area. Specifically, we note the outcome for each sample in the evaluation set and compute the top 3 similar outcomes from the training set using PubMed-BERT [153] embedding similarity. For each drug in the top-3 labels, we

define the likelihood-weighted prior as the abundance of this drug in the subset of the training set positive samples. Then, for each outcome in the evaluation set, each sample (both positive and negative) is scored by the mean of likelihood-weighted prior to the two drugs. This ensures that the baseline considers the abundance of the drug pairs in the evaluation set with the closest safety outcomes in the training set.

5 Research Applications of MADRIGAL

Each DrugBank safety outcomes are annotated with one of nine organs, namely “blood” (hematological), “heart” (cardiovascular), “liver” (hepatic), “kidney” (renal), “gastrointestinal”, “endocrine”, “urinary”, “immune”, “lung”, or otherwise “others/general”. Organs with less than five occurrences (“urinary”, “immune”, “lung”) are not considered in all organ-level analyses. 7 out of 158 safety outcomes, including “adverse effects, decrease”, “cardiotoxicity, decrease”, “hypertension, decrease”, “hypoglycemia, decrease”, “hypotension, decrease”, “nephrotoxicity, decrease”, and “therapeutic efficacy, increase” are considered as potentially beneficial safety outcomes and are thus excluded from all safety-oriented analyses.

5.1 Drug-Induced Effects on Liver, Heart and QT Prolongation

For each drug (drug A) in each dataset, we query the model trained on the DrugBank safety dataset with the input of the form (drug A, drug A, outcome) and obtain scores across all outcomes. For each outcome, we then obtain the normalized rank of drug A by ranking the score among all scores of this outcome produced by 11,601 DrugBank small molecule drugs or novel compounds in our data using the same query format, before normalizing to [0,1].

When correlating our model predictions with annotations in each dataset, since the organ where the toxicity is measured differs, we also make sure the outcomes we consider for our model match such organs (Supplementary Table S1). Specifically, for the DILI (liver) dataset, we obtain predictions from our model with all liver-related outcomes (“excretion rate, increase | serum level, decrease | efficacy, decrease”, “liver damage, increase”, “liver enzyme elevations, increase”, “metabolism, decrease”, and “metabolism, increase”); for the DICT (cardiovascular) dataset, we obtain predictions from our model with all heart-related outcomes (in total, 44 outcomes); and for the DIQTA (QTc prolongation), we obtain predictions from our model with all QTc prolongation-related outcomes (“QTc prolongation, decrease”, “QTc prolongation, hypotension, increase”, “QTc prolongation, increase”, “QTc prolongation, torsade de pointes, cardiotoxicity, increase”). For DILI and DIQTA, we correlate annotations with predictions for each outcome individually; for DICT, due to the large number of outcomes, we correlate

annotations with the average of the highest five predictions across 44 heart-related outcomes.

5.2 Transporter, Carrier, and Enzyme-Mediated Outcomes

We identify safety outcomes in the DrugBank dataset that are potentially transporter-mediated, including “absorption, decrease”, “absorption, decrease | serum level, decrease | efficacy, decrease”, “absorption, increase | serum level, increase | adverse effects, increase”, “excretion rate, decrease | serum level, increase”, “excretion rate, increase | serum level, decrease | efficacy, decrease”, “excretion, decrease”, “excretion, increase”, “serum level of the active metabolites, decrease”, “serum level of the active metabolites, decrease | efficacy, decrease”, “serum level of the active metabolites, increase”, “serum level, decrease”, “serum level, increase”. Among them, “excretion rate, decrease | serum level, increase”, “excretion, decrease”, “serum level of the active metabolites, increase”, “serum level, decrease”, and “serum level, increase” are considered as safety outcomes that are relevant to increase in serum concentration as explored in [57]. We also identified safety outcomes in the DrugBank dataset that are potentially carrier-mediated, including “absorption, decrease”, “absorption, decrease | serum level, decrease | efficacy, decrease”, “absorption, increase | serum level, increase | adverse effects, increase”, “bioavailability, decrease”, “bioavailability, increase”, “protein binding, decrease”, “serum level, decrease”, “serum level, increase”. Similarly, potential enzyme-mediated safety outcomes include “bioavailability, decrease”, “bioavailability, increase”, “metabolism, decrease”, “metabolism, increase”, “protein binding, decrease”, “serum level of the active metabolites, decrease”, “serum level of the active metabolites, decrease | efficacy, decrease”, “serum level of the active metabolites, increase”.

To examine identified transporter-mediated DDIs validated in [57], we first query the model to obtain normalized ranks for the above safety outcomes that are relevant to the increase in serum concentration between doxycycline and each of digoxin, warfarin, tacrolimus, and levetiracetam. Piracetam is a positive control because it is structurally similar to levetiracetam with a side chain modification. It is known to interact with doxycycline, leading to a decrease in excretion and thus, increase in serum concentration. The maximum of the five normalized ranks is presented for each drug pair. Since each drug can interact with many other substrates of their respective transporter (BCRP and MRP2 here), we also calculate two additional values: (1) the quantile of the maximum normalized rank among all pairs of the form (doxycycline, X), and (2) the quantile of the maximum normalized rank among all pairs of the form (digoxin, X), (warfarin, X), (tacrolimus, X), or (levetiracetam, X), calculated individually for each drug, where X is any other DrugBank compound we curate.

To systematically compare the maximum normalized rank of transporter-mediated, carrier-mediated, and enzyme-mediated outcomes among drug pairs with and without overlap in their transporter, carrier, and enzyme profiles, respectively, we consider all drug pairs between drugs with respective profiles available in DrugBank and partition them into two groups, depending on whether or not the two drugs’ profiles overlap. The maximum normalized rank of each safety outcome group is then taken for each drug pair and aggregated according to the drug pair grouping.

Finally, drugs that share each specific transporter are paired and queried to the model to probe into the potential outcomes mediated by individual transporters. The median across all such drug pairs is then taken to rank the relevance of each safety outcome. The signs of outcomes are neutralized. Representative carriers, enzymes, and targets with many drugs sharing them are taken as controls, with the outcomes ranked similarly.

5.3 Cancer Combination Therapies

We consider PARPi’s annotated with at least one outcome and have at least five samples in the organ. This left us with the following PARPis: olaparib, talazoparib, and rucaparib. However, the combination safety dataset lacks data for other PARPis, so we cannot analyze them precisely.

To validate the prediction of the model with clinical knowledge about the neutropenia of PARPi combinations, the following safety outcomes are considered to be neutropenia-related outcomes: “neutropenia, increase”, “cytopenia, increase”, “myelosuppression, anemia, severe leukopenia, increase”, and “neutropenia, thrombocytopenia, increase”. To obtain a summary statistics of each PARPi’s general safety profile about interactions with other drugs, we combine each PARPi with all non-PARPi cancer drugs we curate and take the average of the highest three normalized ranks for each organ for each drug pair, representing the potential level of organ-specific safety concern of each drug pair. Here, for each outcome, normalized ranks are computed by ranking MADRIGAL-predicted scores of each drug pair among scores of all possible drug combinations between DrugBank small molecule compounds in our dataset for this outcome, before normalizing to [0,1]. These drug pair scores are taken directly to plot barplot or boxplot, and the median is taken across these scores for each PARPi and each organ to generate a heatmap.

As a control for all PARPi’s, in relevant analyses, we also include the following drug pairs from [79]:

- FDA-approved drug combinations (decomposed into pairs).

- FDA-approved drug combinations (decomposed into pairs) where at least one of the two drugs is on our curated cancer drug list.
- Clinically investigated drug combinations (decomposed into pairs). These two categories are indistinguishable from the current dataset.

Their scores are calculated in a way similar to PARPi combinations.

5.4 Type 2 Diabetes Comorbidities

We consider the outcomes in Supplementary Table S6 relevant for myocardial infarction and stroke. We then query MADRIGAL with pairs composed of pioglitazone or rosiglitazone and all other T2D drugs before taking the mean across all pairs of such drugs for each outcome related to myocardial infarction or stroke.

For hyperkalemia analysis, we consider “hyperkalemia, increase”, “hypotension, hyperkalemia, nephrotoxicity, increase”, “renal failure, hyperkalemia, hypertension, increase”, and “renal failure, hypotension, hyperkalemia, increase” as hyperkalemia-related outcomes. We then query the model with pairs composed of each HF drug with all T2D drugs. We take the maximum value across the above four outcomes as the safety score, representing each drug pair’s level of hyperkalemia-specific safety concern. For each MoA group of HF drugs, all drug pairs containing an HF drug within the group are considered when plotting the point plot, using the geometric mean as the estimator.

To generate a safety profile for each MASH drug or clinical candidate when combined with T2D drugs or clinical candidates, we first take the average of the highest five normalized ranks for each pair (MASH drug or candidate, T2D drug or candidate). Then, for each MASH drug or clinical candidate, we take the lowest five drug pairs containing it with such scores. This effectively gives us a scalar score for each MASH drug or clinical candidate, representing the (worst) safety profile of the best possible combinations with T2D drugs containing it.

5.5 MASH Combination Therapies

For MASH drug combinations currently under clinical investigation, we first manually annotate them to be either “efficacy” or “safety” based on descriptions of the rationales of developing such drug combinations in existing literature [84, 85, 108]. We then obtain the average of the highest five normalized ranks. In addition, for each such combination, we take all drug pairs with aligned MoA pairs and calculate the average of the highest five normalized ranks, treating those as rational “background” safety for the combination.

5.6 BeatAML

We used principal component analysis (PCA) to reduce the dimension of gene expression data from 22783 to 150, which retains 90.3% of variance. We binary encode somatic mutation data, considering only pathogenic or potentially pathogenic mutations, and filter out those genes with less than three mutations across all patients. We then used multiple correspondence analysis (MCA) to reduce the dimension of the somatic mutation data from 447 to 30, which retains 93.0% of variance. We also keep clinical attributes with less than 10% missingness and impute with either the most frequent or mean values, depending on whether the attribute is categorical or numeric. We exclude technical and administrative attributes and attributes about patient information after specimen collection. After filtering, the following attributes are kept: “gender”, “ageAtDiagnosis”, “priorMalignancyNonMyeloid”, “cumulativeChemo”, “priorMalignancyRadiationTx”, “priorMDS”, “priorMDSMoreThanTwoMths”, “priorMDSMPN”, “priorMDSMPNMoreThanTwoMths”, “priorMPN”, “priorMPNMoreThanTwoMths”, “riskGroup”, “specificDxAtAcquisition”, “ageAtSpecimenAcquisition”, “specimenGroups”, “specimenType”, “FLT3_ITDCall”, “NPM1Call”, “priorTreatmentTypeCount”, “priorTreatmentRegimenCount”, “priorTreatmentStageCount”.

To adapt MADRIGAL for personalized drug combination synergy prediction, we first use frozen MADRIGAL encoders trained with the DrugBank combination safety dataset to generate drug embeddings. Then, we adopt a symmetric bilinear decoder to fuse the two drug embeddings. We concatenate the fused output with dimension-reduced gene expression, somatic mutation data, and clinical attributes before feeding into an MLP, which is trained from scratch to predict binary labels of whether or not drugs combinations are synergistic for the patient, defined above in Methods Sec. 1.9. For each MADRIGAL model (trained with five seeds), we used five seeds to train the bilinear decoder and the MLP for at most 200 epochs, leading to 25 models evaluated for each group. For simplicity, we do not perform hyperparameter tuning. The model’s hyperparameters are the bilinear decoder output dimension = 128, MLP hidden dimensions = [256, 128], MLP dropout = 0.2, and learning rate = 0.001. The AdamW optimizer is used for training.

We used AUROC as our primary performance metric. We calculated AUROC in two distinct ways: (1) Patient-centric AUROC: For each patient, we computed the AUROC across all drug combination predictions, then averaged these values over all patients. (2) Drug-centric AUROC: For each drug combination, we computed the AUROC across predictions from different patients, and then averaged these values. This dual approach provides complementary insights into the model’s performance at both the patient level and the drug combination level.

5.7 Patient-derived xenograft encyclopedia

Given the small number of samples available, we use PCA to reduce the dimension of gene expression data from 20,684 down to 25, which retains 64.5% of variance. We binary encoded somatic mutation data, considering only pathogenic or potentially pathogenic mutations, and filtered out genes with fewer than three mutations in all patients. We then used MCA to reduce the dimension of the somatic mutation data from 2935 to 25, which retains 63.7% of variance.

To adapt MADRIGAL for personalized drug combination synergy prediction, we first use frozen MADRIGAL encoders trained with the DrugBank dataset to generate drug embeddings as with the BeatAML dataset. Then, given the small amount of data available, we adopt a simple element-wise max to fuse the two drug embeddings and concatenate the fused output with dimension-reduced gene expression and somatic mutation data before feeding into a random forest regressor. For each MADRIGAL weight (trained with five seeds), we again use five seeds to train the random forest regressor, leading to 25 models. For simplicity, we do not conduct hyperparameter tuning. The hyperparameters of the model are: number of estimators (trees) = 1000, criterion to measure the quality of a split = `friedman-MSE`, maximum depth of the tree = `Not set`, minimum number of samples required to split an internal node = 2. Prediction cutoff of responsiveness is set to -20, aligning with [41] (complete response, partial response vs. stable disease, progressive disease according to the mRECIST criteria), for plotting stratified Kaplan-Meier survival estimates.

References

1. Palmer, A. C. & Sorger, P. K. Combination cancer therapy can confer benefit via patient-to-patient variability without drug additivity or synergy. *Cell* **171**, 1678–1691.e13 (2017).
2. Jin, H., Wang, L. & Bernards, R. Rational combinations of targeted cancer therapies: background, advances and challenges. *Nature Reviews Drug Discovery* **22**, 213–234 (2023).
3. Ratziu, V. & Charlton, M. Rational combination therapy for NASH: Insights from clinical trials and error. *Journal of Hepatology* **78**, 1073–1079 (2023).
4. Colombel, J. F. *et al.* Infliximab, azathioprine, or combination therapy for crohn's disease. *New England journal of medicine* **362**, 1383–1395 (2010).
5. Doki, Y. *et al.* Nivolumab combination therapy in advanced esophageal squamous-cell carcinoma. *New England Journal of Medicine* **386**, 449–462 (2022).
6. Murphy, C. C. *et al.* Polypharmacy and patterns of prescription medication use among cancer survivors. *Cancer* **124**, 2850–2857 (2018).
7. Menditto, E. *et al.* Patterns of multimorbidity and polypharmacy in young and adult population: Systematic associations among chronic diseases and drugs using factor analysis. *PLoS One* **14**, e0210701 (2019).
8. Csoti, I., Herbst, H., Urban, P., Woitalla, D. & Wüllner, U. Polypharmacy in parkinson's disease: risks and benefits with little evidence. *Journal of Neural Transmission* **126**, 871–878 (2019).
9. Sun, Y. *et al.* Combining genomic and network characteristics for extended capability in predicting synergistic drugs for cancer. *Nature Communications* **6**, 8481 (2015).
10. Sun, W., Sanderson, P. E. & Zheng, W. Drug combination therapy increases successful drug repositioning. *Drug Discovery Today* **21**, 1189–1195 (2016).
11. AI's potential to accelerate drug discovery needs a reality check. *Nature* **622**, 217–217 (2023).
12. Huang, K. *et al.* Therapeutics data commons: Machine learning datasets and tasks for drug discovery and development. In Vanschoren, J. & Yeung, S. (eds.) *Proceedings of the Neural Information Processing Systems Track on Datasets and Benchmarks 1, NeurIPS Datasets and Benchmarks 2021, December 2021, virtual* (2021).
13. Swanson, K. *et al.* ADMET-AI: a machine learning admet platform for evaluation of large-scale chemical libraries. *Bioinformatics* **40**, btae416 (2024).
14. Karunajeewa, H. A. *et al.* A trial of combination antimalarial therapies in children from papua new guinea. *New England Journal of Medicine* **359**, 2545–2557 (2008).
15. Jaaks, P. *et al.* Effective drug combinations in breast, colon and pancreatic cancer cells. *Nature* **603**, 166–173 (2022).

16. Subramanian, A. *et al.* A next generation Connectivity Map: L1000 platform and the first 1,000,000 profiles. *Cell* **171**, 1437–1452.e17 (2017).
17. Corsello, S. M. *et al.* Discovering the anticancer potential of non-oncology drugs by systematic viability profiling. *Nature Cancer* **1**, 235–248 (2020).
18. Lamb, J. *et al.* The Connectivity Map: Using gene-expression signatures to connect small molecules, genes, and disease. *Science* **313**, 1929–1935 (2006).
19. Cohen, A. A. *et al.* Dynamic proteomics of individual cancer cells in response to a drug. *Science* **322**, 1511–1516 (2008).
20. Molinelli, E. J. *et al.* Perturbation biology: Inferring signaling networks in cellular systems. *PLoS Computational Biology* **9**, e1003290 (2013).
21. Lukáčin, M. & Bollenbach, T. Emergent gene expression responses to drug combinations predict higher-order drug interactions. *Cell Systems* **9**, 423–433.e3 (2019).
22. Wu, L. *et al.* A hybrid deep forest-based method for predicting synergistic drug combinations. *Cell Reports Methods* **3**, 100411 (2023).
23. Iorio, F. *et al.* Discovery of drug mode of action and drug repositioning from transcriptional responses. *Proceedings of the National Academy of Sciences* **107**, 14621–14626 (2010).
24. Jang, G. *et al.* Predicting mechanism of action of novel compounds using compound structure and transcriptomic signature coembedding. *Bioinformatics* **37**, i376–i382 (2021).
25. Pham, T.-H., Qiu, Y., Zeng, J., Xie, L. & Zhang, P. A deep learning framework for high-throughput mechanism-driven phenotype compound screening and its application to COVID-19 drug repurposing. *Nature Machine Intelligence* **3**, 247–257 (2021).
26. Pham, T.-H. *et al.* Chemical-induced gene expression ranking and its application to pancreatic cancer drug repurposing. *Patterns* **3**, 100441 (2022).
27. Barretina, J. *et al.* The cancer cell line encyclopedia enables predictive modelling of anticancer drug sensitivity. *Nature* **483**, 603–607 (2012).
28. Rees, M. G. *et al.* Correlating chemical sensitivity and basal gene expression reveals mechanism of action. *Nature Chemical Biology* **12**, 109–116 (2016).
29. Pan, J. *et al.* Sparse dictionary learning recovers pleiotropy from human cell fitness screens. *Cell Systems* **13**, 286–303.e10 (2022).
30. Oberlick, E. M. *et al.* Small-molecule and crispr screening converge to reveal receptor tyrosine kinase dependencies in pediatric rhabdoid tumors. *Cell Reports* **28**, 2331–2344.e8 (2019).
31. Corsello, S. M. *et al.* Discovering the anticancer potential of non-oncology drugs by systematic viability profiling. *Nature Cancer* **1**, 235–248 (2020).

32. Raghavan, S. *et al.* Microenvironment drives cell state, plasticity, and drug response in pancreatic cancer. *Cell* **184**, 6119–6137.e26 (2021).
33. Hahn, W. C. *et al.* An expanded universe of cancer targets. *Cell* **184**, 1142–1155 (2021).
34. Wu, N., Jastrzebski, S., Cho, K. & Geras, K. J. Characterizing and overcoming the greedy nature of learning in multi-modal deep neural networks. In Chaudhuri, K. *et al.* (eds.) *International Conference on Machine Learning, ICML 2022, 17-23 July 2022, Baltimore, Maryland, USA*, vol. 162 of *Proceedings of Machine Learning Research*, 24043–24055 (PMLR, 2022).
35. Huang, Y., Lin, J., Zhou, C., Yang, H. & Huang, L. Modality competition: What makes joint training of multi-modal network fail in deep learning? (provably). In Chaudhuri, K. *et al.* (eds.) *International Conference on Machine Learning, ICML 2022, 17-23 July 2022, Baltimore, Maryland, USA*, vol. 162 of *Proceedings of Machine Learning Research*, 9226–9259 (PMLR, 2022).
36. Ektefaie, Y., Dasoulas, G., Noori, A., Farhat, M. & Zitnik, M. Multimodal learning with graphs. *Nature Machine Intelligence* **5**, 340–350 (2023).
37. Radford, A. *et al.* Learning transferable visual models from natural language supervision. In Meila, M. & Zhang, T. (eds.) *Proceedings of the 38th International Conference on Machine Learning, ICML 2021, 18-24 July 2021, Virtual Event*, vol. 139 of *Proceedings of Machine Learning Research*, 8748–8763 (PMLR, 2021).
38. Yuan, X. *et al.* Multimodal contrastive training for visual representation learning. In *IEEE Conference on Computer Vision and Pattern Recognition, CVPR 2021, virtual, June 19-25, 2021*, 6995–7004 (Computer Vision Foundation / IEEE, 2021).
39. Bottomly, D. *et al.* Integrative analysis of drug response and clinical outcome in acute myeloid leukemia. *Cancer Cell* **40**, 850–864.e9 (2022).
40. Eide, C. A. *et al.* Clinical correlates of venetoclax-based combination sensitivities to augment acute myeloid leukemia therapy. *Blood Cancer Discovery* **4**, 452–467 (2023).
41. Gao, H. *et al.* High-throughput screening using patient-derived tumor xenografts to predict clinical trial drug response. *Nature Medicine* **21**, 1318–1325 (2015).
42. Nagrani, A. *et al.* Attention bottlenecks for multimodal fusion. In Ranzato, M., Beygelzimer, A., Dauphin, Y., Liang, P. & Vaughan, J. W. (eds.) *Advances in Neural Information Processing Systems*, vol. 34, 14200–14213 (Curran Associates, Inc., 2021).
43. Recasens, A. *et al.* Zorro: the masked multimodal transformer. *CoRR* **abs/2301.09595** (2023). [2301.09595](#).
44. Jaegle, A. *et al.* Perceiver IO: A general architecture for structured inputs & outputs. In *The Tenth International Conference on Learning Representations, ICLR 2022, Virtual Event, April 25-29, 2022* (2022).
45. Tatonetti, N. P., Ye, P. P., Daneshjou, R. & Altman, R. B. Data-driven prediction of drug effects and interactions. *Science Translational Medicine* **4** (2012).

46. Wishart, D. S. *et al.* Drugbank 5.0: a major update to the drugbank database for 2018. *Nucleic Acids Research* **46**, D1074–D1082 (2018).
47. Zitnik, M., Agrawal, M. & Leskovec, J. Modeling polypharmacy side effects with graph convolutional networks. *Bioinformatics* **34**, i457–i466 (2018).
48. Kim, Y., Ryu, J. Y., Kim, H. U. & Lee, S. Y. Computational prediction of interactions between paxlovid and prescription drugs. *Proceedings of the National Academy of Sciences* **120**, e2221857120 (2023).
49. Huang, K., Xiao, C., Hoang, T., Glass, L. & Sun, J. Caster: Predicting drug interactions with chemical substructure representation. *Proceedings of the AAAI Conference on Artificial Intelligence* **34**, 702–709 (2020).
50. Nyamabo, A. K., Yu, H., Liu, Z. & Shi, J.-Y. Drug–drug interaction prediction with learnable size-adaptive molecular substructures. *Briefings in Bioinformatics* **23**, bbab441 (2022).
51. Su, X., Hu, L., You, Z., Hu, P. & Zhao, B. Attention-based knowledge graph representation learning for predicting drug-drug interactions. *Briefings in Bioinformatics* **23**, bbac140 (2022).
52. Chen, Y. *et al.* MUFFIN: Multi-scale feature fusion for drug-drug interaction prediction. *Bioinformatics* **37**, 2651–2658 (2021).
53. Su, X., Hu, P., You, Z.-H., Yu, P. S. & Hu, L. Dual-channel learning framework for drug-drug interaction prediction via relation-aware heterogeneous graph transformer. *Proceedings of the AAAI Conference on Artificial Intelligence* **38**, 249–256 (2024).
54. Chen, M. *et al.* Dilirank: the largest reference drug list ranked by the risk for developing drug-induced liver injury in humans. *Drug Discovery Today* **21**, 648–653 (2016).
55. Qu, Y., Li, T., Liu, Z., Li, D. & Tong, W. DICTrank: The largest reference list of 1318 human drugs ranked by risk of drug-induced cardiotoxicity using FDA labeling. *Drug Discovery Today* **28**, 103770 (2023).
56. Li, S., Xu, Z., Guo, M., Li, M. & Wen, Z. Drug-induced qt prolongation atlas (DIQTA) for enhancing cardiotoxicity management. *Drug Discovery Today* **27**, 831–837 (2022).
57. Shi, Y. *et al.* Screening oral drugs for their interactions with the intestinal transportome via porcine tissue explants and machine learning. *Nature Biomedical Engineering* **8**, 278–290 (2024).
58. Galetin, A. *et al.* Membrane transporters in drug development and as determinants of precision medicine. *Nature Reviews Drug Discovery* **23**, 255–280 (2024).
59. The International Transporter Consortium *et al.* Membrane transporters in drug development. *Nature Reviews Drug Discovery* **9**, 215–236 (2010).
60. Meric-Bernstam, F. *et al.* National cancer institute combination therapy platform trial with molecular analysis for therapy choice (ComboMATCH). *Clinical Cancer Research* **29**, 1412–1422 (2023).

61. Huang, A., Garraway, L. A., Ashworth, A. & Weber, B. Synthetic lethality as an engine for cancer drug target discovery. *Nature Reviews Drug Discovery* **19**, 23–38 (2020).
62. Bang, Y.-J. *et al.* Olaparib in combination with paclitaxel in patients with advanced gastric cancer who have progressed following first-line therapy (GOLD): a double-blind, randomised, placebo-controlled, phase 3 trial. *The Lancet Oncology* **18**, 1637–1651 (2017).
63. Saad, F. *et al.* Olaparib plus abiraterone versus placebo plus abiraterone in metastatic castration-resistant prostate cancer (PROpel): final prespecified overall survival results of a randomised, double-blind, phase 3 trial. *The Lancet Oncology* **24**, 1094–1108 (2023).
64. AstraZeneca Pharmaceuticals LP. Label: Lynparza - olaparib tablet, film coated. Online; accessed Apr 2024.
65. AstraZeneca. Lynparza in combination with abiraterone approved in the EU as 1st-line treatment for patients with metastatic castration-resistant prostate cancer (2022). Online; accessed Apr 2024. Available from <https://wwwastrazeneca.com/media-centre/press-releases/2022/lynparza-approved-in-eu-for-prostate-cancer.html>.
66. Küçükosmanoglu, A. *et al.* A real-world toxicity atlas shows that adverse events of combination therapies commonly result in additive interactions. *Clinical Cancer Research* **30**, 1685–1695 (2024).
67. Ring, A. *et al.* Olaparib and ceralasertib (AZD6738) in patients with triple-negative advanced breast cancer: Results from cohort E of the plasmaMATCH trial (CRUK/15/010). *Clinical Cancer Research* **29**, 4751–4759 (2023).
68. Wethington, S. L. *et al.* Combination ATR (ceralasertib) and PARP (olaparib) inhibitor (CAPRI) trial in acquired PARP inhibitor–resistant homologous recombination–deficient ovarian cancer. *Clinical Cancer Research* **29**, 2800–2807 (2023).
69. Simpkins, F. *et al.* Combination ATR and PARP inhibitor (CAPRI): A phase 2 study of ceralasertib plus olaparib in patients with recurrent, platinum-sensitive epithelial ovarian cancer (cohort A). *Journal of Clinical Oncology* **42**, 5510–5510 (2024).
70. Tutt, A. *et al.* 161O VIOLETTE: Randomised phase II study of olaparib (ola) + cerasertib (cer) or adavosertib (ada) vs ola alone in patients (pts) with metastatic triple-negative breast cancer (mTNBC). *Annals of Oncology* **33**, S194–S195 (2022).
71. Barash, M., Reich, K. A. & Rademaker, D. Lidocaine-induced methemoglobinemia: A clinical reminder. *Journal of Osteopathic Medicine* **115**, 94–98 (2015).
72. Guay, J. Methemoglobinemia related to local anesthetics: A summary of 242 episodes. *Anesthesia & Analgesia* **108**, 837–845 (2009).
73. Pfizer Laboratories Div Pfizer Inc. Label: Talzenna - talazoparib capsule, liquid filled. Online; accessed Apr 2024.
74. Clovis Oncology, Inc. Label: Rubraca - rucaparib tablet, film coated. Online; accessed Apr 2024.
75. LaFargue, C. J., Dal Molin, G. Z., Sood, A. K. & Coleman, R. L. Exploring and comparing adverse events between PARP inhibitors. *The Lancet Oncology* **20**, e15–e28 (2019).

76. Litton, J. K. *et al.* Talazoparib in patients with advanced breast cancer and a germline *brca* mutation. *New England Journal of Medicine* **379**, 753–763 (2018).
77. Bruin, M. A. C., Sonke, G. S., Beijnen, J. H. & Huitema, A. D. R. Pharmacokinetics and pharmacodynamics of parp inhibitors in oncology. *Clinical Pharmacokinetics* **61**, 1649–1675 (2022).
78. Bhamidipati, D., Haro-Silerio, J. I., Yap, T. A. & Ngoi, N. PARP inhibitors: enhancing efficacy through rational combinations. *British Journal of Cancer* **129**, 904–916 (2023).
79. Shtar, G., Azulay, L., Nizri, O., Rokach, L. & Shapira, B. CDCDB: A large and continuously updated drug combination database. *Scientific Data* **9**, 263 (2022).
80. Langenberg, C., Hingorani, A. D. & Whitty, C. J. M. Biological and functional multimorbidity—from mechanisms to management. *Nature Medicine* **29**, 1649–1657 (2023).
81. Ong, K. L. *et al.* Global, regional, and national burden of diabetes from 1990 to 2021, with projections of prevalence to 2050: a systematic analysis for the global burden of disease study 2021. *The Lancet* **402**, 203–234 (2023).
82. Younossi, Z. *et al.* Global burden of NAFLD and NASH: trends, predictions, risk factors and prevention. *Nature Reviews Gastroenterology & Hepatology* **15**, 11–20 (2018).
83. Del Prato, S. Rational combination therapy for type 2 diabetes. *The Lancet Diabetes & Endocrinology* **7**, 328–329 (2019).
84. Tilg, H., Byrne, C. D. & Targher, G. NASH drug treatment development: challenges and lessons. *The Lancet Gastroenterology & Hepatology* **8**, 943–954 (2023).
85. Harrison, S. A., Allen, A. M., Dubourg, J., Noureddin, M. & Alkhouri, N. Challenges and opportunities in NASH drug development. *Nature Medicine* **29**, 562–573 (2023).
86. Younossi, Z. M. & Henry, L. Understanding the burden of nonalcoholic fatty liver disease: Time for action. *Diabetes Spectrum* **37**, 9–19 (2024).
87. Dharmalingam, M. & Yamas, P. Nonalcoholic fatty liver disease and type 2 diabetes mellitus. *Indian Journal of Endocrinology and Metabolism* **22**, 421 (2018).
88. Office of the Commissioner, FDA. FDA approves first treatment for patients with liver scarring due to fatty liver disease (2024). Available from <https://www.fda.gov/news-events/press-announcements/fda-approves-first-treatment-patients-liver-scarring-due-fatty-liver-disease>.
89. Avram, S. *et al.* Drugcentral 2023 extends human clinical data and integrates veterinary drugs. *Nucleic Acids Research* **51**, D1276–D1287 (2023).
90. Chandak, P., Huang, K. & Zitnik, M. Building a knowledge graph to enable precision medicine. *Scientific Data* **10**, 67 (2023).
91. Diabetes Teaching Center at the University of California, San Francisco. Table of medications. Online; accessed Sep 2023. Available from <https://dtc.ucsf.edu/types-of-diabetes/type2/treatment-of-type-2-diabetes/medications-and-therapies/type-2-non-insulin-therapies/table-of-medications/>.

92. Mayo Clinic Staff. Diabetes treatment: Medications for type 2 diabetes. Online; accessed Sep 2023. Available from <https://www.mayoclinic.org/diseases-conditions/type-2-diabetes/in-depth/diabetes-treatment/art-20051004>.
93. Cleveland Clinic. Oral diabetes medications. Online; accessed Sep 2023. Available from <https://my.clevelandclinic.org/health/articles/12070-oral-diabetes-medications>.
94. Nissen, S. E. & Wolski, K. Effect of rosiglitazone on the risk of myocardial infarction and death from cardiovascular causes. *New England Journal of Medicine* **356**, 2457–2471 (2007).
95. Weinstein, J., Girard, L.-P., Lepage, S., McKelvie, R. S. & Tennankore, K. Prevention and management of hyperkalemia in patients treated with renin–angiotensin–aldosterone system inhibitors. *CMAJ: Canadian Medical Association Journal* **193**, E1836–E1841 (2021).
96. Neuen, B. L. *et al.* Sodium-glucose cotransporter 2 inhibitors and risk of hyperkalemia in people with type 2 diabetes: A meta-analysis of individual participant data from randomized, controlled trials. *Circulation* **145**, 1460–1470 (2022).
97. Oshima, A., Imamura, T., Narang, N. & Kinugawa, K. Management of hyperkalemia in chronic heart failure using sodium zirconium cyclosilicate. *Clinical Cardiology* **44**, 1272–1275 (2021).
98. Imamura, T. *et al.* Combination therapy using sodium zirconium cyclosilicate and a mineralocorticoid receptor antagonist in patients with heart failure and hyperkalemia. *Internal Medicine* **60**, 2093–2095 (2021).
99. Kosiborod, M. N. *et al.* Sodium zirconium cyclosilicate for management of hyperkalemia during spironolactone optimization in patients with heart failure. *Journal of the American College of Cardiology* S0735109724104305 (2024).
100. Desai, A. S. *et al.* Incidence and predictors of hyperkalemia in patients with heart failure. *Journal of the American College of Cardiology* **50**, 1959–1966 (2007).
101. Heerspink, H. J. *et al.* Dapagliflozin in patients with chronic kidney disease. *New England Journal of Medicine* **383**, 1436–1446 (2020).
102. Lin, H.-J. *et al.* Risk of CKD among patients with dm taking diuretics or SGLT2i: a retrospective cohort study in taiwan. *BMC Pharmacology and Toxicology* **25**, 24 (2024).
103. Harrison, S. A., Loomba, R., Dubourg, J., Ratziu, V. & Noureddin, M. Clinical trial landscape in NASH. *Clinical Gastroenterology and Hepatology* **21**, 2001–2014 (2023).
104. Kowdley, K. V. *et al.* Efficacy and safety of elafibranor in primary biliary cholangitis. *New England Journal of Medicine* **390**, 795–805 (2024).
105. Harrison, S. A. *et al.* Resmetirom for nonalcoholic fatty liver disease: a randomized, double-blind, placebo-controlled phase 3 trial. *Nature Medicine* **29**, 2919–2928 (2023).
106. Sanyal, A. J. *et al.* Tropifexor for nonalcoholic steatohepatitis: an adaptive, randomized, placebo-controlled phase 2a/b trial. *Nature Medicine* **29**, 392–400 (2023).

107. Alkhouri, N., Lawitz, E., Noureddin, M., DeFronzo, R. & Shulman, G. I. GS-0976 (firsocostat): an investigational liver-directed acetyl-CoA carboxylase (ACC) inhibitor for the treatment of non-alcoholic steatohepatitis (NASH). *Expert Opinion on Investigational Drugs* **29**, 135–141 (2020).
108. Suri, J., Borja, S. & Lim, J. K. Combination strategies for pharmacologic treatment of non-alcoholic steatohepatitis. *World Journal of Gastroenterology* **28**, 5129–5140 (2022).
109. Sicklick, J. K. *et al.* Molecular profiling of cancer patients enables personalized combination therapy: The I-PREDICT study. *Nature Medicine* **25**, 744–750 (2019).
110. Kather, J. N., Ferber, D., Wiest, I. C., Gilbert, S. & Truhn, D. Large language models could make natural language again the universal interface of healthcare. *Nature Medicine* 1–3 (2024).
111. Juhi, A. *et al.* The capability of chatgpt in predicting and explaining common drug-drug interactions. *Cureus* (2023).
112. Li, T. *et al.* Cancergpt for few shot drug pair synergy prediction using large pretrained language models. *npj Digital Medicine* **7**, 40 (2024).
113. Lambert, B. L., Lin, S.-J. & Tan, H. Designing safe drug names. *Drug Safety* **28**, 495–512 (2005).
114. Kenagy, J. W. & Stein, G. C. Naming, labeling, and packaging of pharmaceuticals. *American Journal of Health-System Pharmacy* **58**, 2033–2041 (2001).
115. Gallifant, J. *et al.* Language models are surprisingly fragile to drug names in biomedical benchmarks. In Al-Onaizan, Y., Bansal, M. & Chen, Y. (eds.) *Findings of the Association for Computational Linguistics: EMNLP 2024, Miami, Florida, USA, November 12-16, 2024*, 12448–12465 (Association for Computational Linguistics, 2024).
116. Mitchell, D. C. *et al.* A proteome-wide atlas of drug mechanism of action. *Nature Biotechnology* **41**, 845–857 (2023).
117. Dent, R. A. *et al.* Phase i trial of the oral PARP inhibitor olaparib in combination with paclitaxel for first-or second-line treatment of patients with metastatic triple-negative breast cancer. *Breast Cancer Research* **15**, 1–8 (2013).
118. Dent, R. *et al.* Safety and efficacy of the oral PARP inhibitor olaparib (AZD2281) in combination with paclitaxel for the first-or second-line treatment of patients with metastatic triple-negative breast cancer: Results from the safety cohort of a phase I/II multicenter trial. *Journal of Clinical Oncology* **28**, 1018–1018 (2010).
119. Vaduganathan, M. *et al.* SGLT2 inhibitors in patients with heart failure: a comprehensive meta-analysis of five randomised controlled trials. *The Lancet* **400**, 757–767 (2022).
120. Younis, I. R. *et al.* Pharmacokinetics and safety of firsocostat, an acetyl-coenzyme a carboxylase inhibitor, in participants with mild, moderate, and severe hepatic impairment. *The Journal of Clinical Pharmacology* **64**, 878–886 (2024).

121. Wu, X. *et al.* Niraparib maintenance therapy in patients with platinum-sensitive recurrent ovarian cancer using an individualized starting dose (NORA): a randomized, double-blind, placebo-controlled phase III trial. *Annals of Oncology* **32**, 512–521 (2021).
122. Zhang, C., Peng, K., Liu, Q., Huang, Q. & Liu, T. Adavosertib and beyond: Biomarkers, drug combination and toxicity of wee1 inhibitors. *Critical Reviews in Oncology/Hematology* **193**, 104233 (2024).
123. Queen, O. *et al.* ProCyon: A multimodal foundation model for protein phenotypes. *bioRxiv* (2024).
124. Su, X. *et al.* Knowledge graph based agent for complex, knowledge-intensive QA in medicine. *CoRR* **abs/2410.04660** (2024). [2410.04660](#).
125. Ochoa, D. *et al.* The next-generation open targets platform: reimagined, redesigned, rebuilt. *Nucleic Acids Research* **51**, D1353–D1359 (2023).
126. Jiang, A. Q. *et al.* Mistral 7b. *CoRR* **abs/2310.06825** (2023). [2310.06825](#).
127. Gosh, M., Maruo, K., Tada, K. & Hirakawa, A. Utilization of chi-square statistics for screening adverse drug-drug interactions in spontaneous reporting systems. *European Journal of Clinical Pharmacology* **73**, 779–786 (2017).
128. Noguchi, Y., Tachi, T. & Teramachi, H. Review of statistical methodologies for detecting drug–drug interactions using spontaneous reporting systems. *Frontiers in Pharmacology* **10**, 1319 (2019).
129. Landrum, G. *et al.* rdkit/rdkit: 2022_03_5 (q1 2022) release (2022).
130. Zhu, J. *et al.* Prediction of drug efficacy from transcriptional profiles with deep learning. *Nature Biotechnology* **39**, 1444–1452 (2021).
131. Lim, N. & Pavlidis, P. Evaluation of connectivity map shows limited reproducibility in drug repositioning. *Scientific Reports* **11**, 17624 (2021).
132. Zhu, J. *et al.* Prediction of drug efficacy from transcriptional profiles with deep learning. *Nature Biotechnology* **39**, 1444–1452 (2021).
133. Zheng, C. & Xu, R. Large-scale mining disease comorbidity relationships from post-market drug adverse events surveillance data. *BMC Bioinformatics* **19** (2018).
134. Klimek, P., Kautzky-Willer, A., Chmiel, A., Schiller-Fruhwirth, I. & Thurner, S. Quantification of diabetes comorbidity risks across life using nation-wide big claims data. *PLoS computational biology* **11**, e1004125 (2015).
135. Pantziarka, P., Capistrano I, R., De Potter, A., Vandeborne, L. & Bouche, G. An open access database of licensed cancer drugs. *Frontiers in Pharmacology* **12**, 627574 (2021).
136. Synapse by Patsnap. Global innovative drug intelligence. Online; accessed January 2024.
137. Hu, Z., Dong, Y., Wang, K. & Sun, Y. Heterogeneous graph transformer. In *Proceedings of The Web Conference 2020*, 2704–2710 (ACM, Taipei Taiwan, 2020).

138. Xu, K., Hu, W., Leskovec, J. & Jegelka, S. How powerful are graph neural networks? In *7th International Conference on Learning Representations, ICLR 2019, New Orleans, LA, USA, May 6-9, 2019* (2019).
139. Hetzel, L. *et al.* Predicting cellular responses to novel drug perturbations at a single-cell resolution. In Koyejo, S. *et al.* (eds.) *Advances in Neural Information Processing Systems 35: Annual Conference on Neural Information Processing Systems 2022, NeurIPS 2022, New Orleans, LA, USA, November 28 - December 9, 2022* (2022).
140. Wang, Y. *et al.* Pubchem's bioassay database. *Nucleic acids research* **40**, D400–D412 (2012).
141. Wu, Z. *et al.* Moleculenet: a benchmark for molecular machine learning. *Chemical science* **9**, 513–530 (2018).
142. Bank, D., Koenigstein, N. & Giryes, R. Autoencoders. *CoRR* **abs/2003.05991** (2020). [2003.05991](#).
143. van den Oord, A., Li, Y. & Vinyals, O. Representation learning with contrastive predictive coding. *CoRR* **abs/1807.03748** (2018). [1807.03748](#).
144. Chen, T., Kornblith, S., Norouzi, M. & Hinton, G. A simple framework for contrastive learning of visual representations. In *Proceedings of the 37th International Conference on Machine Learning*, 1597–1607 (PMLR, 2020).
145. Poole, B., Ozair, S., van den Oord, A., Alemi, A. A. & Tucker, G. On variational bounds of mutual information. In Chaudhuri, K. & Salakhutdinov, R. (eds.) *Proceedings of the 36th International Conference on Machine Learning, ICML 2019, 9-15 June 2019, Long Beach, California, USA*, vol. 97 of *Proceedings of Machine Learning Research*, 5171–5180 (PMLR, 2019).
146. Tsai, Y.-H. H. *et al.* Multimodal transformer for unaligned multimodal language sequences. In *Proceedings of the 57th Annual Meeting of the Association for Computational Linguistics*, 6558–6569 (Association for Computational Linguistics, Florence, Italy, 2019).
147. Li, J. *et al.* Align before fuse: Vision and language representation learning with momentum distillation. In Ranzato, M., Beygelzimer, A., Dauphin, Y. N., Liang, P. & Vaughan, J. W. (eds.) *Advances in Neural Information Processing Systems 34: Annual Conference on Neural Information Processing Systems 2021, NeurIPS 2021, December 6-14, 2021, virtual*, 9694–9705 (2021).
148. Biewald, L. Experiment tracking with weights and biases (2020). Software available from [wandb.com](#).
149. Paszke, A. *et al.* Pytorch: An imperative style, high-performance deep learning library. In *Advances in Neural Information Processing Systems 32*, 8024–8035 (Curran Associates, Inc., 2019).
150. Pedregosa, F. *et al.* Scikit-learn: Machine learning in python. *Journal of Machine Learning Research* **12**, 2825–2830 (2011).

151. Ryu, J. Y., Kim, H. U. & Lee, S. Y. Deep learning improves prediction of drug-drug and drug-food interactions. *Proceedings of the National Academy of Sciences* **115**, E4304–E4311 (2018).
152. Ding, B. *et al.* Data augmentation using LLMs: Data perspectives, learning paradigms and challenges. In Ku, L.-W., Martins, A. & Srikumar, V. (eds.) *Findings of the Association for Computational Linguistics ACL 2024*, 1679–1705 (Association for Computational Linguistics, Bangkok, Thailand and virtual meeting, 2024).
153. Gu, Y. *et al.* Domain-specific language model pretraining for biomedical natural language processing. *ACM Transactions on Computing for Healthcare* **3**, 2:1–2:23 (2022).